A&A 517, A56 (2010)
DOI: 10.1051/0004-6361/200913679

Astronomy & Astrophysics

Class I and Class II methanol masers in high-mass star-forming regions⋆

F. Fontani[1,2], R. Cesaroni[3], and R. S. Furuya[4]

[1] ESO, Karl Schwarzschild Str. 2, 85748 Garching bei München, Germany
[2] Institut de Radio-Astronomie Millimétrique, 300 rue de la Piscine, Domaine Universitaire, 38406 Saint Martin d'Hères, France
e-mail: fontani@iram.fr
[3] INAF-Osservatorio Astrofisico di Arcetri, L.go E. Fermi 5, 50125 Firenze, Italy
[4] Subaru Telescope, National Astronomical Observatory of Japan, 650 North A'ohoku Place, Hilo, HI 96720, USA

Received 16 November 2009 / Accepted 20 April 2010

ABSTRACT

Context. Among the tracers of the earliest phases in the massive star formation process, methanol masers have gained increasing importance. The phenomenological distinction between Class I and II methanol masers is based on their spatial association with objects such as jets, cores, and ultracompact HII regions, but is also believed to correspond to different pumping mechanisms: radiation for Class II masers, collisions for Class I masers.

Aims. We surveyed a large sample of massive star-forming regions in Class I and II methanol masers. The sample consists of 296 sources, divided into two groups named *high* and *low* according to their [25–12] and [60–12] IRAS colours. Previous studies indicate that the two groups may contain similar sources in different evolutionary stages, with the *high* sources representing the more evolved stages. Therefore, the sample can be used to assess a sequence for the occurrence of Class I and II methanol masers during the evolution of a massive star-forming region.

Methods. We observed the 6 GHz (Class II) CH_3OH maser with the Effelsberg 100-m telescope, and the 44 GHz and 95 GHz (Class I) CH_3OH masers with the Nobeyama 45-m telescope.

Results. We detected 55 sources in the Class II line (39 *high* and 16 *low*, 12 new detections); 27 sources in the 44 GHz Class I line (19 *high* and 8 *low*, 17 new detections); 11 sources in the 95 GHz Class I line (eight *high* and three *low*, all except one are new detections). The detection rate of Class II masers decreases with the distance of the source (as expected), whereas that of Class I masers peaks at ∼5 kpc. This could be due to the Class I maser spots being spread over a region $\lesssim$1 pc, comparable to the telescope beam diameter at a distance of ∼5 kpc. We also find that the two Class I lines have similar spectral shapes at 44 GHz and 95 GHz, which confirms that they have the same origin.

Conclusions. Our statistical analysis shows that the ratio between the detection rates of Class II and Class I methanol masers is basically the same in *high* and *low* sources. Therefore, both maser types seem to be equally associated with each evolutionary phase. In contrast, all maser species (including H_2O) have about three times higher detection rates in *high* than in *low* sources. This could indicate that the phenomena from which all masers originate become progressively more active with time during the earliest evolutionary phases of a high-mass star-forming region.

Key words. stars: formation – ISM: molecules – masers

1. Introduction

Maser lines of water (H_2O), hydroxyl (OH), and methanol (CH_3OH) are commonly detected towards regions of high-mass star-formation (e.g. Comoretto et al. 1990; Menten 1991; Kurtz et al. 2000; Pestalozzi et al. 2005). Among these, methanol masers are the most recently discovered, and their place in the star-formation process is still not well understood. Menten (1991) suggested to classify methanol masers into two groups, Class I and Class II. The latter typically coincide in position with hot molecular cores, ultracompact (UC) HII regions, OH masers and near-IR sources (e.g. Minier et al. 2001; Ellingsen et al. 2006) and are believed to be radiatively pumped (Sobolev et al. 2007, and references therein; Cragg et al. 2005). In contrast, Class I masers are also found in massive star-forming regions, but usually offset (∼0.1–1 pc) from other masers, UC HII regions, and bright infrared sources. They seem to be collisionally pumped (Cragg et al. 1992) at the interface between molecular outflows/jets and the quiescent ambient material (Plambeck & Menten 1990). This scenario is supported by observations that reveal a coincidence between Class I methanol masers at 44 GHz and molecular shock tracers (Kurtz et al. 2004; Voronkov et al. 2006).

Even though both species are believed to trace the earliest phases of the massive star-formation process, it is still not clear whether any physical relation exists among them. Slysh et al. (1994) claim an anticorrelation between the intensity of Class I and II methanol masers in the same star-forming region. On the other hand, Ellingsen (2005) searched for Class I masers at 95 GHz towards a sample of known 6 GHz Class II masers and could not find any (anti)correlation between the two. It is also poorly understood whether a relationship exists between the occurrence of Class I and II masers and the evolution of the corresponding massive star-forming region. Van der Walt (2005) estimated a lifetime of the 6 GHz Class II methanol maser of a few 10^4 yrs, thus covering a consistent part of the early life of a massive star. Ellingsen (2006) compared the infrared (GLIMPSE) colours of sources containing Class II methanol masers with or without a Class I methanol maser, and found

⋆ Appendices are only available in electronic form at http://www.aanda.org

that those associated with Class I masers have redder GLIMPSE colours, suggesting that the sources hosting Class I masers are less evolved (see also Breen et al. 2010). However, until now an evolutionary sequence of methanol masers occurence has not been well established, partly because Class I masers are less studied and models for some Class I lines show that their excitation is very sensitive to the physical properties of the environment (Pratap et al. 2008).

To investigate a sequence for the occurrence of Class I and II methanol masers along the evolution of a massive star-forming region, one needs to study large samples of high-mass young stellar objects (YSOs) believed to be in different evolutionary stages. A large sample of massive YSO candidates with this property was identified by Palla et al. (1991): the sources, all with $\delta \geq -30°$, were selected on the basis of their high luminosities ($>10^3\ L_\odot$) and far-infrared (FIR) colours typical of dense molecular clumps. These have been divided into two subsamples based on the IRAS colours[1]: sources with $[25-12] > 0.57$ and $[60-12] > 1.3$ were named *high*, the others *low*. The threshold was taken from Wood & Churchwell (1998), who suggested that UC HII regions have IRAS colours above these limits. Palla et al. (1991) searched for 22 GHz H_2O masers towards *high* and *low* sources, and found a higher detection rate in *high* sources. In the last decade a series of studies aimed at investigating the environment associated with these sources (association with ammonia cores, centimetre and (sub-)millimetre continuum emission, ^{12}CO outflows: Molinari et al. 1996, 1998a, 2000; Brand et al. 2001; Zhang et al. 2001, 2005) indicated that *low* and *high* sources are massive stars in a very early evolutionary stage, with the *low* group dominated by the youngest sources. Two prototypical examples of *high* and *low* objects are IRAS 20126+4104 (Cesaroni et al. 1997, 1999) and IRAS 23385+6053, respectively (Molinari et al. 1998b; Fontani et al. 2004; Molinari et al. 2008).

We have searched for 6 GHz (Class II), 44 GHz (Class I) and 95 GHz (Class I) CH_3OH maser emission in the *high* and *low* sources of the Palla et al. (1991) sample with the aim to find a possible evolutionary sequence for the occurrence of the different masers. The observations were made with the Effelsberg 100-m telescope (at 6 GHz) and Nobeyama 45-m telescope (at 44 and 95 GHz). In Sect. 2 we give an overview of the observations performed and of the data reduction procedure adopted. The results are presented in Sect. 3 and discussed in Sect. 4. A summary of the main findings is given in Sect. 5.

2. Observations and data reduction

2.1. Effelsberg 100-m telescope observations and data reduction

The 5_1-6_0 A$^+$ Class II methanol maser line at 6.6685192 GHz was observed with the Effelsberg 100-m antenna towards 296 sources (149 *high* and 147 *low*; see Table B.1) in May 2003. These consist of all the 260 sources selected by Palla et al. (1991), plus 36 sources with FIR colours characteristic of *high* and *low* sources but rejected by Palla et al. (1991) because associated with known HII regions. Data were obtained using two spectral windows corresponding to the right- (RCP) and left- (LCP) circular polarization. Each spectral window had a ~500 km s^{-1} bandwidth with a spectral resolution of ~0.11 km s^{-1} (4096 channels). For sources previously detected in ammonia by Molinari et al. (1996), we centred the windows at the local standard of rest (LSR) velocity, $V_{\rm LSR}$, obtained from the NH_3 observations. For the other sources the bandwidth was centred at 0 km s^{-1}. The half power beam width at the frequency of the (5_1-6_0 A$^+$) methanol line is ~120″. Because the two polarisations had remarkably different system temperatures (45 K for the LCP and 120 K for the RCP) due to a technical problem, we used only the LCP spectra in the analysis. The conversion factor between main beam brightness temperature and flux density is 1.45 Jy/K. The spectra have a typical 3σ rms of ~0.15 Jy, comparable to the high-sensitivity survey of 6 GHz methanol masers performed by Caswell et al. (2010). The pointing was checked towards W3OH and 3C 123, and the pointing accuracy was always better than 20″. The flux density scale was calibrated by observing NGC7027, whose flux was assumed equal to 5.9 Jy and the flux calibration uncertainty is estimated to be of the order of ±10%.

The data were reduced and analysed by means of the CLASS software, which is part of the GILDAS package[2] developed at IRAM and Observatoire de Grenoble.

2.2. Nobeyama 45-m telescope observations and data reduction

Observations of the Class I 44.069476 GHz (7_0-6_1 A$^+$) and 95.169489 GHz (8_0-7_1 A$^+$) methanol lines towards 88 of the sources observed in the 6 GHz line were performed with the Nobeyama Radio Observatory (NRO) 45-m telescope in April 2002. The 88 sources were randomly selected among the 260 sources of Palla et al. (1991), depending on the available observing time, and should not have introduced any bias in the sub-sample. We used two SIS receivers simultaneously, centred at the rest frequencies of the lines. The half power beam width was ~38″ at 44 GHz and ~18″ at 95 GHz. The observations were made in position-switching mode. The telescope pointing was checked observing nearby SiO maser sources at 43 GHz; we estimated a pointing accuracy of 3″. The main beam efficiencies were 0.75 and 0.53 at 44 and 95 GHz, respectively. As a backend, we used the AOS-H which provides velocity resolutions of ~0.14 km s^{-1} at 44 GHz and ~0.06 km s^{-1} at 95 GHz. The AOS-H arrays had velocity coverages of 272 km s^{-1} at 44 GHz and 126 km s^{-1} at 95 GHz, and were centred at the same velocity used for the 6 GHz observations. The system temperature was ~300–500 K at 44 GHz, and 700–1300 K at 95 GHz. All the spectra were calibrated with the standard chopper wheel method. Assuming that the telescope beam is Gaussian, the conversion between the main-beam brightness temperature, $T_{\rm MB}$, and flux density, F_ν, is F_ν(Jy) = 2.23 $T_{\rm MB}$(K). We reduced the data using the NEWSTAR package developed by the NRO. Subsequently, the fully reduced spectra were converted into CLASS format for further scientific analysis.

Towards some of the sources observed in the CH_3OH lines, we also obtained spectra of the ammonia (1, 1), (2, 2), and (3, 3) inversion transitions. The details of these NH_3 spectra are not presented in this work; we used these spectra only to derive the systemic LSR velocities, $V_{\rm sys}$, of the sources whose $V_{\rm sys}$ cannot be found in the literature (see Tables B.2 and B.3, and Sect. 4.3).

3. Results

In this section we present the detections in the three lines observed, and the parameters obtained from the fitting procedure described in Sects. 2.1 and 2.2. Spectra of all detected sources

[1] We define the IRAS colours as $[\lambda_1 - \lambda_2] = \log_{10}(F_{\lambda_1}/F_{\lambda_2})$.

[2] The GILDAS software is available at http://www.iram.fr/IRAMFR/GILDAS

Table 1. Sources observed (O), detected (D) and corresponding detection rates (DR) of CH_3OH masers, and H_2O maser at 22 GHz in *high* and *low* sources.

	6 GHz			44 GHz			95 GHz			H_2O	44 GHz / 6 GHz	H_2O / 6 GHz	44 GHz / H_2O
	O	D	DR	O	D	DR	O	D	DR				
high	147	39	27 ± 4%	40	19	48 ± 8%	40	8	20 ± 6%	28 ± 4%	1.8 ± 0.6	1.0 ± 0.3	1.8 ± 0.5
low	149	16	11 ± 3%	48	8	17 ± 5%	48	3	6 ± 3%	9 ± 2%	1.5 ± 0.8	0.8 ± 0.4	1.9 ± 1.0
total	296	55	19 ± 2%	88	27	31 ± 5%	88	11	13 ± 4%				
high/*low*			2.9 ± 1.3			2.5 ± 1.1			3.3 ± 1.4	3.1 ± 1.1	1.2 ± 1.0	1.2 ± 1.0	0.9 ± 0.7

are shown in Appendix A. The spectra are grouped as follows: sources detected in all three lines are shown in Fig. A.1; sources detected only in the 6 GHz and 44 GHz lines are shown in Fig. A.2; sources detected only in the 44 GHz and 95 GHz lines are shown in Fig. A.3; sources detected only in the 6 GHz line are shown in Figs. A.4 and A.4; sources detected only in the 44 GHz line are shown in Fig. A.5. The list of detection and non-detections as well as the main parameters of the lines are tabulated in Appendix B.

3.1. New detections

Our survey has been cross-correlated with catalogues and large surveys of both Class I and II methanol masers. For the 6.7 GHz line, we used the catalogue of Pestalozzi et al. (2005), and the recent works of Cyganowski et al. (2009) and Caswell et al. (2010). For the Class I lines we used the catalogue of Val'tts & Larionov (2007); Chen et al. (2009); Pratap et al. (2008); Cyganowski et al. (2009). We have found 12 new 6.7 GHz methanol masers, 17 new 44 GHz methanol masers (of which three are marginal detections). To our knowledge, all the sources detected in the 95 GHz methanol masers except IRAS 21391+5802 (detected in Val'tts et al. 1995) are new detections.

The new detections are marked in italics in Table B.1.

3.2. Observed sources and detection summary

The observed sources are listed in Table B.1. The IRAS name, the type (*high* = H; *low* = L), and the corresponding equatorial coordinates are reported in Cols. 1 to 4. In Col. 5 we give the velocities used for the observations (see Sect. 2.1). In Cols. 6 to 8 we give the following information: source detected (Y), undetected (N), or not observed (–) in the three CH_3OH lines (6 Ghz in Col. 6, 44 GHz in Col. 7, 95 GHz in Col. 8). For the sake of completeness, we give in Col. 9 the same information for the 22 GHz H_2O maser emission. For this, the information was taken from Palla et al. (1991), Valdettaro et al. (2001), Wouterloot et al. (1993), Henning et al. (1992), and Medicina archival data.

In Fig. 1 we plot a sketch summarising the number of sources in which one, two, or all three lines have been detected. Given that the sample observed in the Class I CH_3OH masers is much smaller than that observed in the other two lines, for the H_2O and Class II CH_3OH masers we also give the number of detected sources that have been *observed* also in the Class I maser (numbers in parentheses in Fig. 1).

The number of sources observed and detected in the three maser species, and the corresponding detection rates, are summarised in Table 1. We also give the same information for the 22 GHz H_2O maser (Col. 11) and some detection rate ratios: 44 GHz/6 GHz (Col. 12), H_2O/6 GHz (Col. 13) and 44 GHz/H_2O (Col. 14). For the Class I CH_3OH maser line, we consider the 44 GHz line only because all sources detected at 95 GHz have also been detected at 44 GHz. One can notice that the detection rates of the Class II masers are comparable to those of H_2O masers both in *high* and *low* sources (respectively, 27% and 28% in *high* sources, 11% and 9% in *low* sources), whereas the Class I masers have a higher detection rate than Class II and H_2O masers in both source types (48% in *high* sources, 17% in *low* sources).

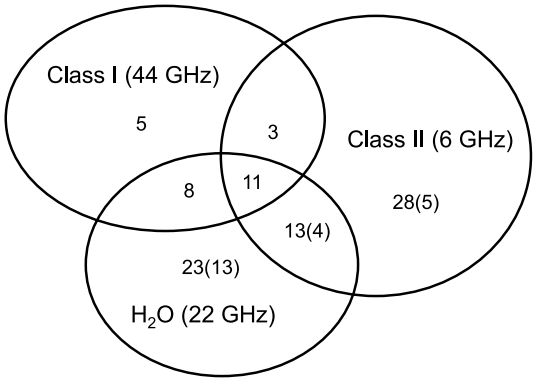

Fig. 1. Sketch showing the number of sources detected in the three maser lines. In parentheses we give the number of sources detected in the 22 GHz H_2O maser and/or in the Class II CH_3OH maser also observed in the Class I (44 GHz) CH_3OH maser.

The *high*/*low* detection ratio given in Table 1 has the purpose to highlight possible differences between the relative occurrence of masers of Class I and II in *high* and *low* sources: The most evident result from Table 1 is that the detection rates in all the masers (Class I, Class II, H_2O) are greater in *high* than in *low* sources. On the other hand, their ratios seem to be independent of the distinction between *high* and *low* (Cols. 12–14). Therefore, our analysis does not reveal any significant difference in the *relative* occurrence of the different masers observed in *high* and *low* sources. We propose an interpretation of this result in Sect. 4.1.

The 95 GHz Class I line has the lowest total detection rate (13%) and all the sources detected in this line have been detected also in the Class I 44 GHz line. We checked whether the different detection rates in the two Class I masers (31% at 44 GHz versus 13% at 95 GHz) could be due to worse signal-to-noise ratio (S/N) at 95 GHz than at 44 GHz. For this purpose, we first estimated the noise level that one should have had in the 44 GHz spectra to achieve the same average S/N as in the 95 GHz spectra: this is 0.7–0.8 Jy. Then we computed the detection rate that we would have achieved at 44 GHz with this noise: this turns out to be 25%, which is still significantly higher than the 13% obtained for the 95 GHz line. Therefore the different detection rates in the two lines cannot be attributed only to the different noise level, but must be due to different intensities of the two masers.

3.3. Parameters of the 6 GHz (Class II) CH_3OH masers

In Table B.2 we list the parameters obtained from Gaussian fits to the 6 GHz maser lines for *high* sources. In Col. 2 we give the systemic velocity (V_{LSR}) of the sources. This was obtained mainly from NH_3 observations[3]. The best-fit parameters are given in Cols. 3 to 6 as follows: integrated intensity (Col. 3); peak velocity (Col. 4); line width at half maximum (Col. 5); peak intensity (Col. 6). The same information is given for *low* sources in Table B.3. As can be seen from the spectra in Figs. A.1–A.4, in the large majority (85%) of the detected sources the emission consists in multiple peaks spread over a well defined velocity range rather than in a single line. Interestingly, only two out of the seven sources with only one line in the spectrum belong to the *high* group. Indeed, 94% of the detected *high* sources have multiple lines, while only 70% of *low* sources do. The line widths are between 0.2 and 0.9 km s^{-1} in the large majority (∼95%) of the lines, and never exceed 1.5 km s^{-1} except in two cases: 18089–1732, and one line in the spectrum of 18048–2019. We believe that in these sources (especially 18089–1732, for which we derive a line width of 10 km s^{-1}) the broad linewidths are due to blending of several narrow lines. This is suggested because that other surveys of this maser transition in similar IRAS sources (Szymczak & Kus 2000) have revealed line widths narrower than 1 km s^{-1} in all cases.

In our survey we find a median flux density peak of ∼15 Jy and a median number of lines per spectrum of 4 (see Tables B.2 and B.3). Among the new detections, only two sources have components with peak flux densities in excess of 6 Jy, IRAS 05480+2545 and IRAS 18024–2119, and 10 out of 12 sources have less than five components.

Walsh et al. (1997) observed a sample of 535 IRAS sources south of $\delta = 0°$ in the 6 GHz CH_3OH maser with the Parkes 64-m telescope. They observed four sources that have also been observed in our survey (18159–1648, 18236–1205, 18265–1517 and 18316–0602), all belonging to the *high* group. We find a good agreement – both in the flux densities of the lines and in the velocity ranges – between the spectra taken with the two telescopes in all sources, except 18236–1205. In 18236–1205, the Parkes 64-m observations show more spectral features and an intensity more than twice the one observed by us with the Effelsberg 100-m telescope. This is likely due to the variability of the maser line. In the sources detected in the Parkes survey, the median value of the flux density peak is ∼13 Jy, and the median number of lines per spectrum (i.e. per source) is 5 (Walsh et al. 1997), consistent with our findings.

3.4. Parameters of the 44 and 95 GHz (Class I) CH_3OH masers

The parameters obtained from Gaussian fits to the spectra observed towards both *high* and *low* sources at 44 GHz, shown in Figs. A.1–A.3 and A.5, are given in Table B.4. The structure of the table is the same as Tables B.2 and B.3, but a letter has been added to the IRAS name to denote if the source belongs to the *high* (H) or *low* (L) sample. Thirteen of the 27 detected objects (i.e. ∼50%) are undetected in the 6 GHz line, among which is the brightest 44 GHz source, 18018–2426. Contrary to the 6 GHz lines, at 44 GHz only eight sources out of the 27 detected show multiple components, and the line widths are generally broader than, or comparable to, 1 km s^{-1}; only 31% of the sources show linewidths below this limit (see Table B.4). In addition, the lines are not very bright on average: except 18018–2426, for which the peak flux is ∼350 Jy, the others have intensities of the order of 1–10 Jy. We did not find any systematic differences between the old and new detections neither in the peak fluxes nor in the line widths.

The relatively broad linewidths suggest either that some of the lines are thermal or that they are the superposition of several blended components. We believe that the second possibility is more likely on the basis of the VLA observations of Kurtz et al. (2004). These authors observed some of our sources with better sensitivity and angular resolution revealing multiple components spread over a velocity range comparable to the line widths measured by us with the Nobeyama 45-m telescope. The sources in common with the survey of Kurtz et al. (2004) are 18144−1723, 18162–1612, 19092+0841, 21307+5049, 21391+5802 and 23385+6053. All of them were also detected in our observations with the sole exception of 21307+5049, which has an intensity peak of ∼1 Jy in the observations of Kurtz et al. (2004). Because this value is higher than the 3σ rms in our observations, the intensity of this maser has probably decreased with time. In 18144–1723, 19092+0841 and 23385+6053 we detect only one line, while Kurtz et al. (2004) detected multiple lines separated by about 2–3 km s^{-1}. This can explain the line widths observed in our study (∼1.5, 5.7 and 3.2 km s^{-1}, respectively). We thus conclude that most of the line widths >1 km s^{-1} are likely due to multiple components having small (≤0.5 km s^{-1}) velocity separations. This is also supported by the study of Slysh et al. (1994), who detected the 44 GHz line in 148 massive young stellar objects similar to those studied in this work, and derived linewidths ≲1 km s^{-1} in the large majority (87%, against our 31%) of the sources.

Finally, in Table B.5 we list the line parameters obtained from Gaussian fits to the spectra at 95 GHz. All sources detected in this line were also detected in the 44 GHz transition (see Table B.1). At 95 GHz, as well as at 44 GHz, 18018–2426 is the brightest source. The line widths are distributed around 1–2 km s^{-1}, and the peak intensities are of the order of 1 Jy, with the above mentioned exception of 18018–2426 (∼50 Jy), suggesting that some of the detected lines might be thermal. In the survey of Kalenskii et al. (1994), the linewidths are similar to those measured in our sources, but the intensities are comparable to or higher than 40 Jy, suggesting maser emission.

At first glance, the spectra of the 44 GHz and 95 GHz masers shown in Figs. A.1 and A.3 indicate that the shape of these two lines are similar in a given source, and clearly different from that of the corresponding 6 GHz maser. To analyse this effect more quantitatively, we normalised each spectrum with respect to the peak intensity and then calculated the quantity $|f_{95\,GHz} - f_{44\,GHz}|/f_{44\,GHz}$, where f_ν indicates the integral under the lines of the normalised spectrum. In Fig. 2 we plot this quantity as a function of the flux integrated under the 44 GHz lines, $F_{44\,GHz}$, for 9 out of the 11 sources detected in both lines. We did not include 18396–0431, because the detection at 44 GHz is very doubtful. We also excluded 21391+5802, for which the 95 and 44 GHz lines have inconsistent velocity ranges. Figure 2 demonstrates that seven sources, i.e. ∼65% of the total, have relative deviations ≤0.3. Even though the number of sources is very low, this result indicates that the two Class I masers have similar

[3] For most sources the velocity is taken from the NH_3 survey by Molinari et al. (1996); for seven sources it is estimated from NH_3 spectra obtained with the Nobeyama 45-m telescope during the same observing run allocated for the observations of the CH_3OH masers (see Sect. 2.2); for the remaining sources we took the systemic velocities from Sridharan et al. (2002); Bronfman et al. (1996, from observations of the CS(2–1) line); Richards et al. (1987) from observations of HCO^+ (1–0); Sunada et al. (2007) and references therein.

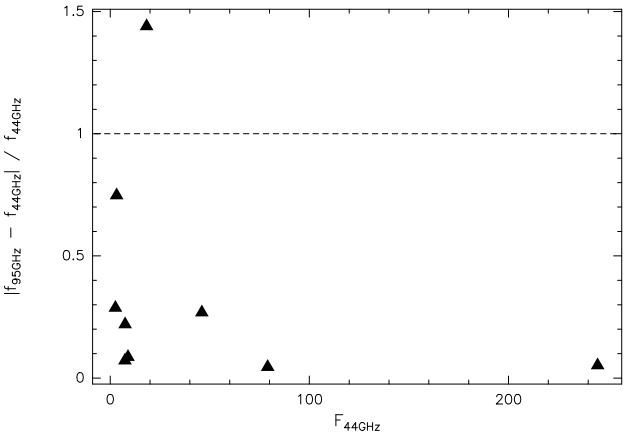

Fig. 2. Relative difference between the integrated intensity of the lines in the normalised spectra (see text) at 95 GHz and 44 GHz, $|f_{95\,\mathrm{GHz}} - f_{44\,\mathrm{GHz}}|/f_{44\,\mathrm{GHz}}$, as a function of the integrated flux $F_{44\,\mathrm{GHz}}$ for 9 out of the 11 sources detected in both lines. We did not include 18396−0431 because it is only marginally detected in the 44 GHz line, and 21391+5802, for which the 95 and 44 GHz lines have inconsistent velocity ranges.

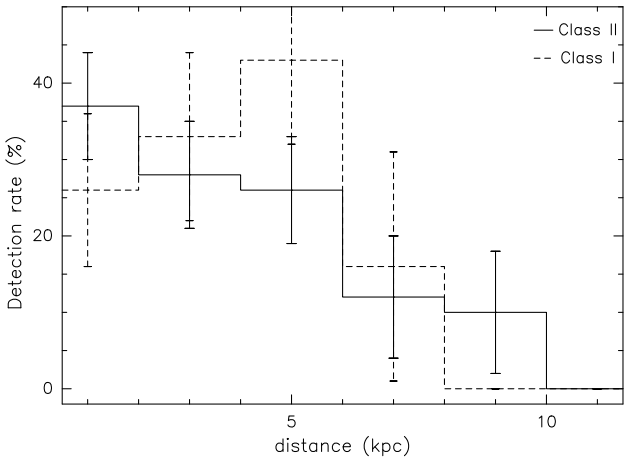

Fig. 3. Distributions of the detection rate for the Class II 6 GHz maser (solid line) and Class I 44 GHz maser (dashed line) as a function of the source distance.

shapes in the majority of the sources detected in both lines, thus confirming the findings of previous studies (e.g. Val'tts et al. 1995).

4. Discussion

An important caveat to be kept in mind when considering our results is that the angular resolution of our observations (18″−120″) corresponds to a maximum linear scale of several parsecs. Regions that large contain a multiplicity of YSOs, possibly in different evolutionary stages, so that it is impossible to associate our findings for a given maser species with a single object. Nevertheless, our results have a *statistical* significance in the sense that they represent the *mean* properties of the whole star-forming region encompassed by the telescope beam. The validity of this approach is demonstrated by the distinction itself between *high* and *low* sources, which is based on the IRAS data, whose resolution is similar to that of our observations. In this regard, we also stress that such a similarity guarantees a consistent comparison between our findings and the source classification based on the IRAS colours.

For these reasons, it is not surprising that we do not find neither a correlation nor an anti-correlation between the intensity of Class I and that of Class II masers. While this might be expected for different maser types associated with single YSOs, any such effect is bound to disappear when multiple sources are observed altogether. On the other hand, one can still use the detection rates described in Sect. 3.2 to draw statistical conclusions on the relative evolutionary phase of the different maser types. This will be done in Sect. 4.1.

Below we will also illustrate and compare properties such as the typical line width and the line velocity dispersion for the different maser types.

4.1. Detection rates: high versus low sources

The most evident result of this work is that for all maser types the detection rates are a factor of ∼3 greater in *high* sources than in *low* sources, which indicates that all types of maser emission in a high-mass star-forming region become more easily excited as evolution proceeds. This conclusion is confirmed because, as noted in Sect. 3.2, the *ratio* between the detection rates of two different maser types does not change significantly from *high* to *low* sources. In other words, all masers appear to evolve in a similar way from the *low* to the *high* phase, because the proportion of detected masers remains the same in *low* and *high* sources.

A possible interpretation of these results is that all phenomena triggering population inversion and hence maser emission (outflow/accretion shocks, hot dust emission, etc.) become more and more prominent during the evolution. Therefore, as time goes on, the number of bipolar outflows, accretion disks, and luminous infrared sources increases in a given star-forming region, thus leading to a corresponding increase of the number of maser sources.

Our findings appear to contradict the suggestion by Ellingsen (2006) that Class I masers are associated with younger sources than those associated with CH_3OH Class II and H_2O masers. However, Ellingsen's claim is admittedly based on a low number of sources and, as stated by the author himself, is rather speculative. A larger number of data with better angular resolution for both methanol maser types will be needed before drawing any conclusion on this issue.

4.2. Detection in Class I and II masers and source distance

In Fig. 3 we plot the detection rates for the CH_3OH masers at 6 GHz (Class II) and 44 GHz (Class I) as a function of the source distance. The kinematic distance was taken from the following papers: Molinari et al. (1996, 2008); Sridharan et al. (2002); Zhang et al. (2005); Sunada et al. (2007). The plot shows that most of the sources detected at 6 GHz have distances between 1 and 5 kpc and the detection rate rapidly decreases with increasing distance. This is an obvious consequence because the closer the source, the higher is the measured flux. However, while the Class II maser detection rate increases all the way to the smallest distances, that of the Class I masers attains a maximum at ∼5 kpc (45% of the sources observed between 4 and 6 kpc are detected) and then decreases for smaller distances, even though the distance distribution of the whole sample peaks at distances lower than ∼5 kpc (see Fig. 3 in Molinari et al. 1996). Our interpretation is that in each source the Class I maser spots are spread over a significantly larger region than that of the Class II maser spots. Consequently, in the closest objects part (or all) of

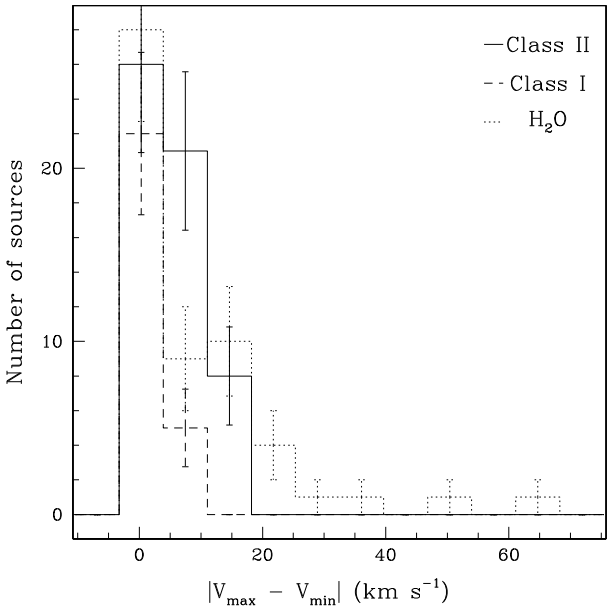

Fig. 4. Distribution of the difference between minimum and maximum line velocities for the Class II 6 GHz (solid line), Class I 44 GHz (dashed line) methanol masers, and of the 22 GHz H_2O maser (dotted line). For spectra with a single line, we plot the measured full width at half maximum.

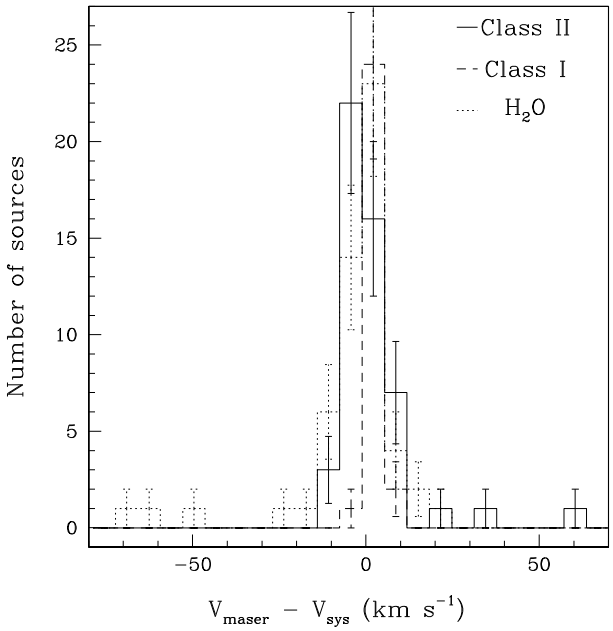

Fig. 5. Distribution of the difference between maser velocity and systemic velocity of the Class II 6 GHz (solid line), Class I 44 GHz (dashed line) methanol masers, and of the 22 GHz H_2O maser (dotted line). For sources with multiple lines, we have taken the velocity of the strongest one.

the Class I spots happen to fall outside the instrumental HPBW. This idea is supported by the fact that – as argued in Sect. 1 – Class I masers are located typically 0.1–1 pc away from the centre of star-formation activity, whereas Class II masers are found closer to it. At 44 GHz the HPBW of the Nobeyama 45-m telescope is ∼38″, which translates into a linear size of ∼0.9 pc at a distance of 5 kpc, consistent with the maximum spread observed in Class I maser spots.

4.3. Velocity ranges in Class I and Class II masers

Figure 4 shows the distribution of the velocity range, derived as the difference between the minimum and maximum velocity peak of the different lines in each spectrum, $|V_{max} - V_{min}|$, for the Class II 6 GHz and Class I 44 GHz CH_3OH masers, and for the sources detected in the 22 GHz H_2O masers by Palla et al. (1991, see their Table 2a) and Valdettaro et al. (2001, Table 1). Out of the 55 sources detected in the H_2O maser line, 44 belong to the Palla et al. (1991) sample. For spectra with a single line we assumed as velocity range the measured full width at half maximum (Col. 5 of Tables B.2–B.4), to be consistent with Palla et al. (1991). The majority of the sources show maser emission of Class I CH_3OH spread over velocity ranges smaller than 6 km s^{-1} (93%), while 60% and ∼64% of the H_2O and Class II maser emission, respectively, have a velocity range smaller than this value, suggesting once more that Class II masers originate from an environment different from that required to excite Class I masers. The distributions of the velocity ranges for Class II and H_2O masers look more similar each other. However, that of the Class II masers extends up to velocity ranges of ∼12 km s^{-1}, whereas the distributions of the Class I and H_2O masers are clearly more peaked at small values: Fig. 4 shows that 21 out of 55 sources (38%) detected in the Class II maser have velocity ranges between ∼6 and ∼12 km s^{-1}, wehreas only 16% and 19% of the sources detected in the H_2O and Class I lines have velocity ranges in this interval. Finally, the largest difference between the maximum and minimum velocities is found in H_2O masers. Indeed, six sources show H_2O emission spread over a velocity range larger than ∼20 km s^{-1}, whereas in all CH_3OH masers the spread is below this limit. In summary, Fig. 4 indicates that there are no clear correlations among the velocity spreads of any of the three maser types.

In Fig. 5 we plot the distribution of the difference between the velocity of the maser, V_{maser}, and the systemic one, V_{sys} once again for the three maser types. Obviously, we did not include sources without available measurements for V_{sys} in Fig. 5. These are: 06291+0421, 17582-2234 and 19045+0813, among the sources detected in the H_2O maser, and 17571-2328 and 19186+1440 (see Tables B.2 and B.3) among those detected in the CH_3OH masers. V_{sys} for the H_2O maser detections was taken from ammonia measurements (Molinari et al. 1996; Valdettaro et al. 2001). For spectra with multiple lines we adopted as V_{maser} that of the peak. The 6 GHz masers show a distribution centred around zero, but the majority of the sources (∼67%) have a separation of ∼5 km s^{-1} or more between the systemic and the peak velocity. On the other hand, for the 44 GHz lines, the distribution is much more peaked around zero and only six sources (22%) have a separation larger than ∼5 km s^{-1}. The distribution of the H_2O maser more closely resembles that of the Class II CH_3OH line, and it shows the largest absolute difference between V_{maser} and V_{sys}. However, the sources with the largest velocity separation have V_{maser} blue-shifted with respect to V_{sys}, while for Class II lines the largest difference is observed in redshifted lines.

Altogether, the results shown in Figs. 4 and 5 suggest that the 44 GHz maser emission is originated in gas with smaller velocity spread and closer to the systemic velocity than the gas in which the other masers are produced. This finding appears in contrast with the belief that Class I masers could be associated with jets/outflow (Plambeck & Menten 1990; Kurtz et al. 2004), unless the jet axis lies very close to the plane of the sky. Before drawing any conclusion, though, one must take into account the

effect of the different noise at 44 and 6 GHz, which can play a significant role in shaping the distribution in Fig. 4. To take this into account, we proceeded as done in Sect. 3.2 for the comparison between the 44 and 95 GHz spectra. The 3σ rms of the Effelsberg 100-m spectra is ∼0.03–0.04 Jy, whereas the one needed to achieve the same average signal to noise ratio as at 44 GHz is ∼2.2 Jy. By inspecting Tables B.2 and B.3 one can see that several lines are below this limit, especially those at the edge of the velocity interval, i.e. those used to calculate $|V_{max} - V_{min}|$. Therefore, the different rms noise at the two frequencies plays an important role in the estimate of $|V_{max} - V_{min}|$. To quantify this effect, we recalculated the histogram in Fig. 4 for the 6 GHz line, excluding the lines fainter than ∼2.2 Jy, and find that the histogram is still slightly wider than that at 44 GHz. In conclusion, we believe that the different distributions for the three maser types correspond to different formation environments, with Class I masers possibly forming in shocks slower than those generating e.g. H_2O masers and/or propagating perpendicular to the line of sight.

5. Summary and conclusions

We have searched for three methanol maser lines (6 GHz Class II, 44 GHz Class I, and 95 GHz Class I) towards a large sample of massive YSOs divided into two groups (*high* and *low*) on the basis of their IRAS colours (Palla et al. 1991). Previous studies indicate that the two groups are in different evolutionary stages, with *high* sources being the more evolved. This work aims to use this sample to test a possible evolutionary sequence in the appearence of Class I and II methanol masers. The main findings of our study are:

- We detected 55 sources in the Class II line (39 *high* and 16 *low*, 12 new detections); 27 sources in the 44 GHz Class I line (19 *high* and 8 *low*, 17 new detections); 11 sources in the 95 GHz Class I line (eight *high* and three *low*, all are new detections except IRAS 21391+5802).
- The detection rates of all the masers observed are higher (by a factor ∼3) in *high* than in *low* sources: the *high*/*low* detection rate ratios are 2.9 ± 1.3 for the Class I 44 GHz line, 3.3 ± 1.6 for the 95 GHz Class I line, and 2.5 ± 1.1 for the Class II line. All these values are similar to those found for H_2O masers, i.e. 3.1 ± 1.1. Going from *low* to *high* sources, we do not find any statistically significant difference in the *relative* occurrence of Class I masers with respect to Class II masers. An analogous result holds for the ratio between the detection rates of CH_3OH and H_2O masers. A possible interpretation is that all maser species analysed in this work evolve similarly during the evolutionary phases corresponding to *high* and *low* sources.
- The detection rate of the Class II masers decreases with the distance of the source, as expected, whereas that of the Class I masers peaks at ∼5 kpc. We interpret this result with Class I maser spots being typically spread over a larger ($\lesssim$1 pc) region than Class II maser spots.
- The spectra in the two Class I masers appear to have similar shapes in seven out of the 11 sources detected in both lines, confirming a common physical origin. Their different detection rates cannot be explained only with the different noise levels at 44 and 95 GHz and we thus conclude that the 95 GHz line is intrinsically fainter.

Acknowledgements. We thank the anonymous referee for the constructive criticism that helped us to shorten, focus, and substantially improve the paper. We are grateful to the Effelsberg and Nobeyama staff for their help during the observations. For part of this work, F.F. acknowledges support by Swiss National Science Foundation grant (PP002 – 110504). The research leading to these results has received funding from the European Community's Seventh Framework Programme (FP7/2007–2013) under grant agreement No. 229517. This work is partially supported by a Grant-in-Aid from the Ministry of Education, Culture, Sports, Science and Technology of Japan (No. 20740113).

References

Brand, J., Cesaroni, R., Palla, F., & Molinari, S. 2001, A&A, 370, 230
Breen, S. L., Ellingsen, S. P., Johnston-Hollitt, M., et al. 2007, MNRAS, 377, 491
Breen, S. L., Ellingsen, S. P., Caswell, J. L., & Lewis, B. E. 2010, 401, 2219
Bronfman, L., Nyman, L.-A., & May, J. 1996, A&AS, 115, 81
Caswell, J. L., Fuller, G. A., Green, J. A., et al. 2010, MNRAS, 404, 1029
Cesaroni, R., Felli, M., Testi, L., Walmsley, C. M., & Olmi, L. 1997, A&A, 325, 725
Cesaroni, R., Felli, M., Jenness, T., et al. 1999, A&A, 345, 949
Chen, X., Ellingsen, S. P., & Shen, Z.-Q. 2009, MNRAS, 396, 1609
Codella, C., & Moscadelli, L. 2000, A&A, 362, 723
Comoretto, G., Palagi, F., Cesaroni, R., et al. 1990, A&AS, 84, 179
Cragg, D., Johns, K., Godfrey, P., & Brown, R. 1992, MNRAS, 259, 203
Cragg, D. M., Sobolev, A. M., & Godfrey, P. D. 2005, MNRAS, 360, 533
Cyganowski, C. J., Brogan, C. L., Hunter, T. R., & Churchwell, E. 2009, ApJ, 702, 1615
Ellingsen, S. P. 2005, MNRAS, 359, 1498
Ellingsen, S. P. 2006, ApJ, 638, 241
Fontani, F., Cesaroni, R., Testi, L., et al. 2004, A&A, 414, 299
Henning, T., Cesaroni, R., Walmsley, M., & Pfau, W. 1992, A&AS, 93, 525
Kalenskii, S. V., Liljestroem, T., Val'tts, I. E., et al. 1994, A&AS, 103, 129
Kurtz, S., Cesaroni, R., Churchwell, E., Hofner, P., & Walmsley, C. M. 2000, Protostars and Planets IV, 299
Kurtz, S., Hofner, P., & Alvarez, C. V. 2004, ApJS, 155, 149
Menten, K. M. 1991, in Atoms, ions and molecules: New results in spectral line astrophysics, ed. A. Haschick, & P. T. P. Ho (San Francisco: ASP), 16, 119
Minier, V., Conway, J. E., & Booth, R. S. 2001, A&A, 369, 278
Molinari, S., Brand, J., Cesaroni, R., & Palla, F. 1996, A&A, 308, 573
Molinari, S., Brand, J., Cesaroni, R., Palla, F., & Palumbo, G. G. C. 1998a, A&A, 336, 339
Molinari, S., Testi, L., Brand, J., Cesaroni, R., & Palla, F. 1998b, ApJ, 505, L39
Molinari, S., Brand, J., Cesaroni, R., & Palla, F. 2000, A&A, 355, 617
Molinari, S., Pezzuto, S., Cesaroni, R., et al. 2008, A&A, 481, 345
Palla, F., Brand, J., Cesaroni, R., Comoretto, G., & Felli, M. 1991, A&A, 246, 249
Pestalozzi, M., Minier, V., & Booth, R. S. 2005, A&A, 432, 737
Plambeck, R. M., & Menten, K. M. 1990, ApJ, 364, 555
Pratap, P., Shute, P. A., Keane, T. C., Battersby, C., & Sterling, S. 2008, AJ, 135, 1718
Richards, P. J., Little, L. T., Heaton, B. D., & Toriseva, M. 1987, MNRAS, 228, 43
Slysh, V. I., Kalenskii, S. V., Valtts, I. E., & Otrupcek, R. 1994, MNRAS, 268, 464
Sobolev, A. M., et al. 2007, Astrophysical Masers and their Environments, Proc. IAU, IAU Symp., 242, 81
Sridharan, T. K., Beuther, H., Schilke, P., Menten, K. M., & Wyrowski, F. 2002, ApJ, 566, 931
Sunada, K., Nakazato, T., Ikeda, N., et al. 2007, PASJ, 59, 1185
Szymczak, M., & Kus, A. J. 2000, A&A, 360, 311
Valdettaro, L., Palla, F., Brand, J., et al. 2001, A&A, 368, 845
Val'tts, I. E., & Larionov, G. M. 2007, ARep, 51, 519
Val'tts, I. E., Dzyura, A. M., Kalenskii, S. V., et al. 1995, AZh, 72, 22
van der Walt, J. 2005, MNRAS, 360, 153
Voronkov, M. A., Brooks, K. J., Sobolev, A. M., et al. 2006, MNRAS, 373, 411
Walsh, A. J., Hyland, A. R., Robinson, G., & Burton, M. G. 1997, MNRAS, 291, 261
Wood, D. O. S., & Churchwell, E. 1989, ApJ, 340, 265
Wouterloot, J. G. A., Brand, J., & Fiegle, K. 1993, A&AS, 98, 589
Zhang, Q., Hunter, T. R., Brand, J., et al. 2001, ApJ, 552, L167
Zhang, Q., Hunter, T. R., Brand, J., et al. 2005, ApJ, 625, 864

Pages 8 to 24 are available in the electronic edition of the journal at http://www.aanda.org

Appendix A: Spectra of detected sources

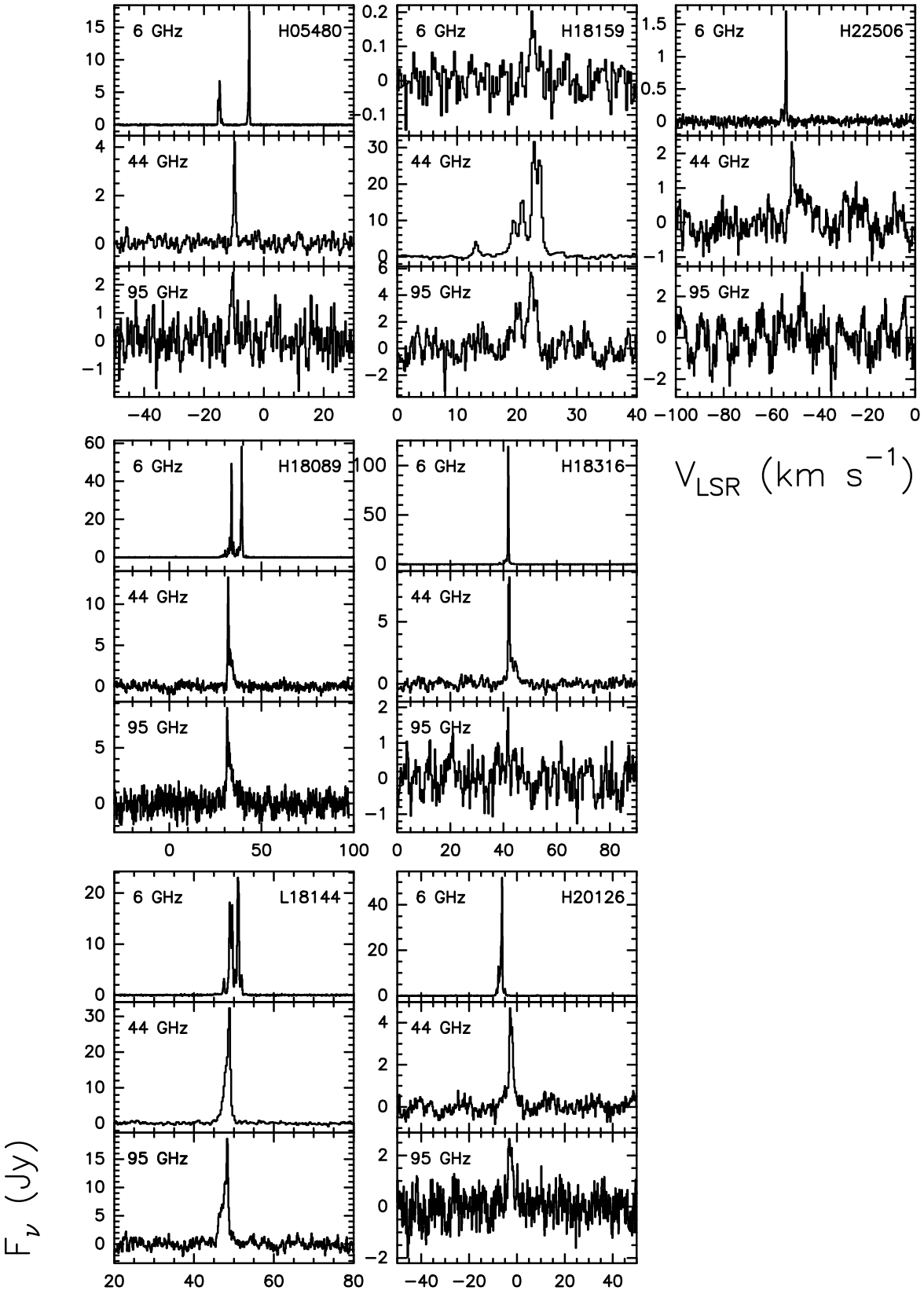

Fig. A.1. Spectra of the three CH_3OH masers (*from top to bottom*: 6 GHz, 44 GHz and 95 GHz) observed towards the nine sources for which all masers have been detected.

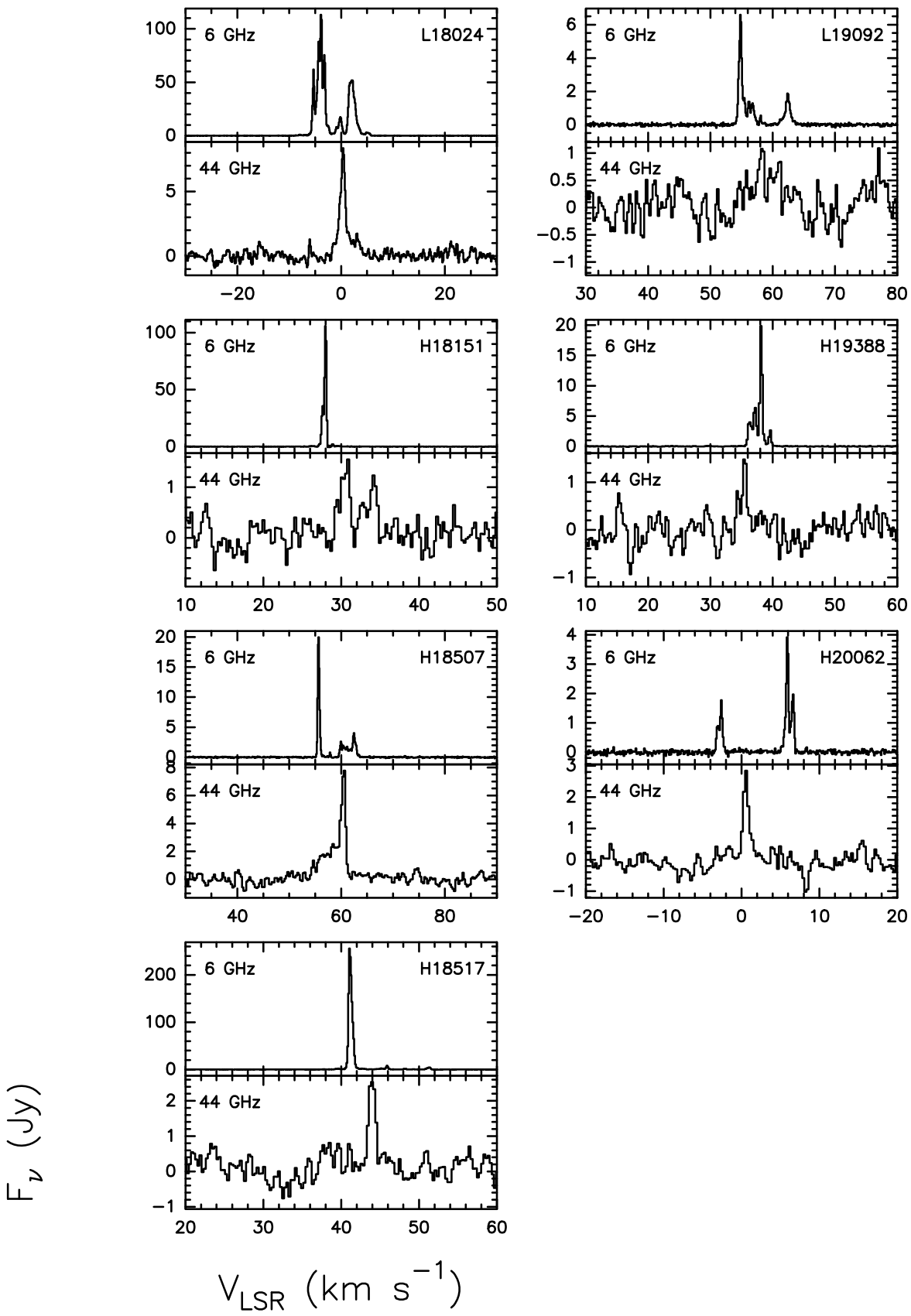

Fig. A.2. Same as Fig. A.1 for sources detected in the 6 GHz and 44 GHz masers.

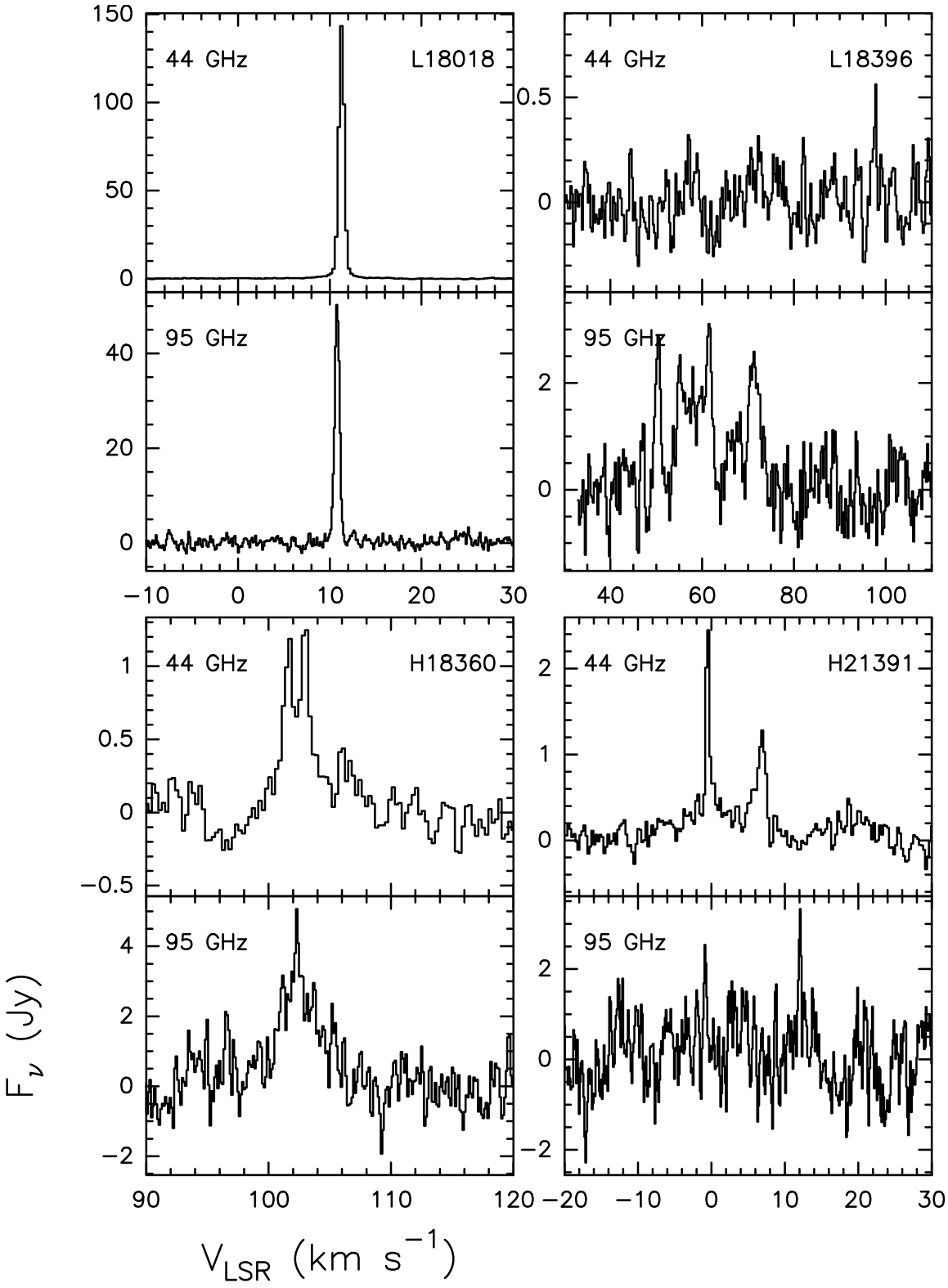

Fig. A.3. Same as Fig. A.1 for sources detected in the 44 GHz and 95 GHz masers.

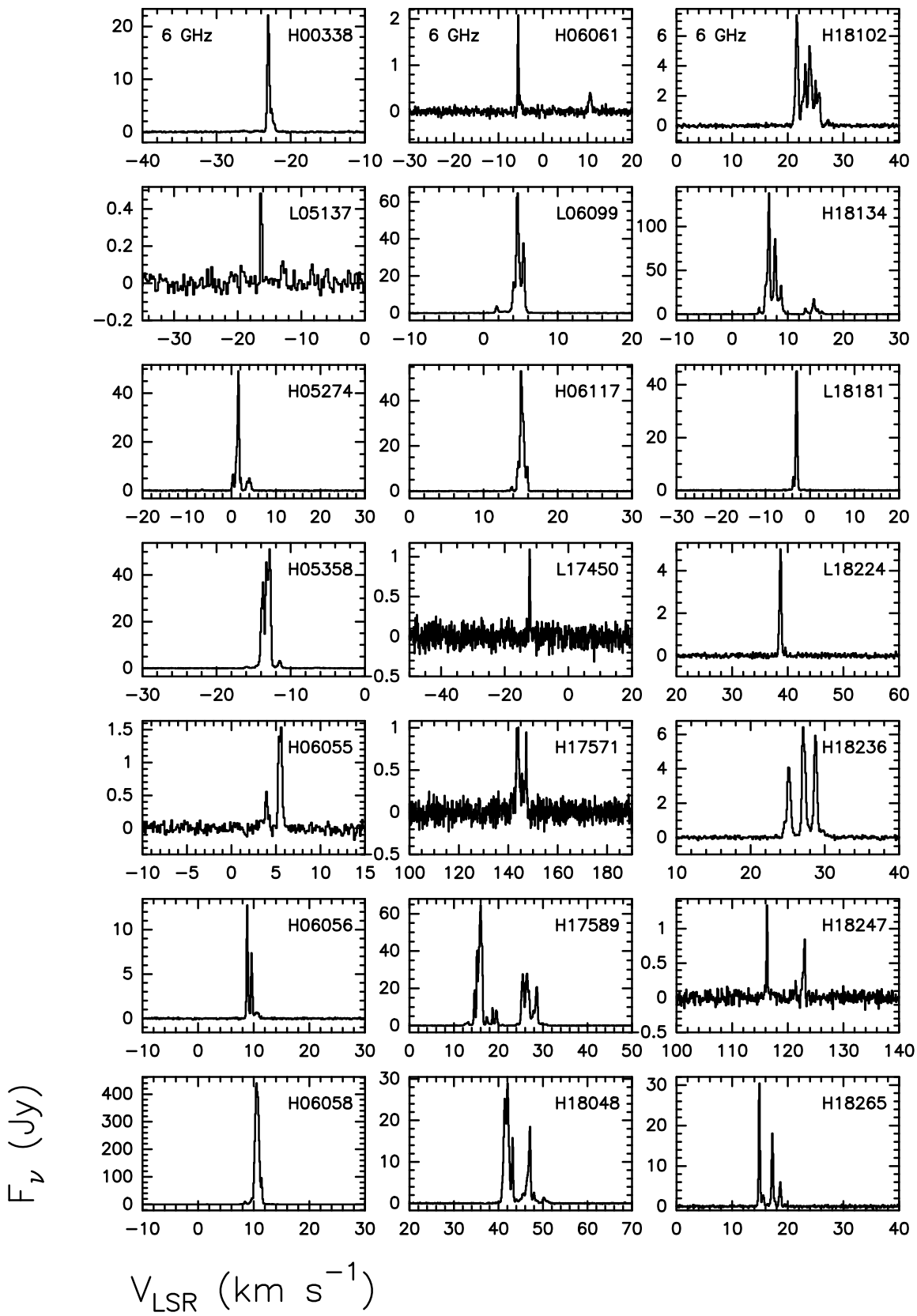

Fig. A.4. Same as Fig. A.1 for sources detected in the 6 GHz maser only.

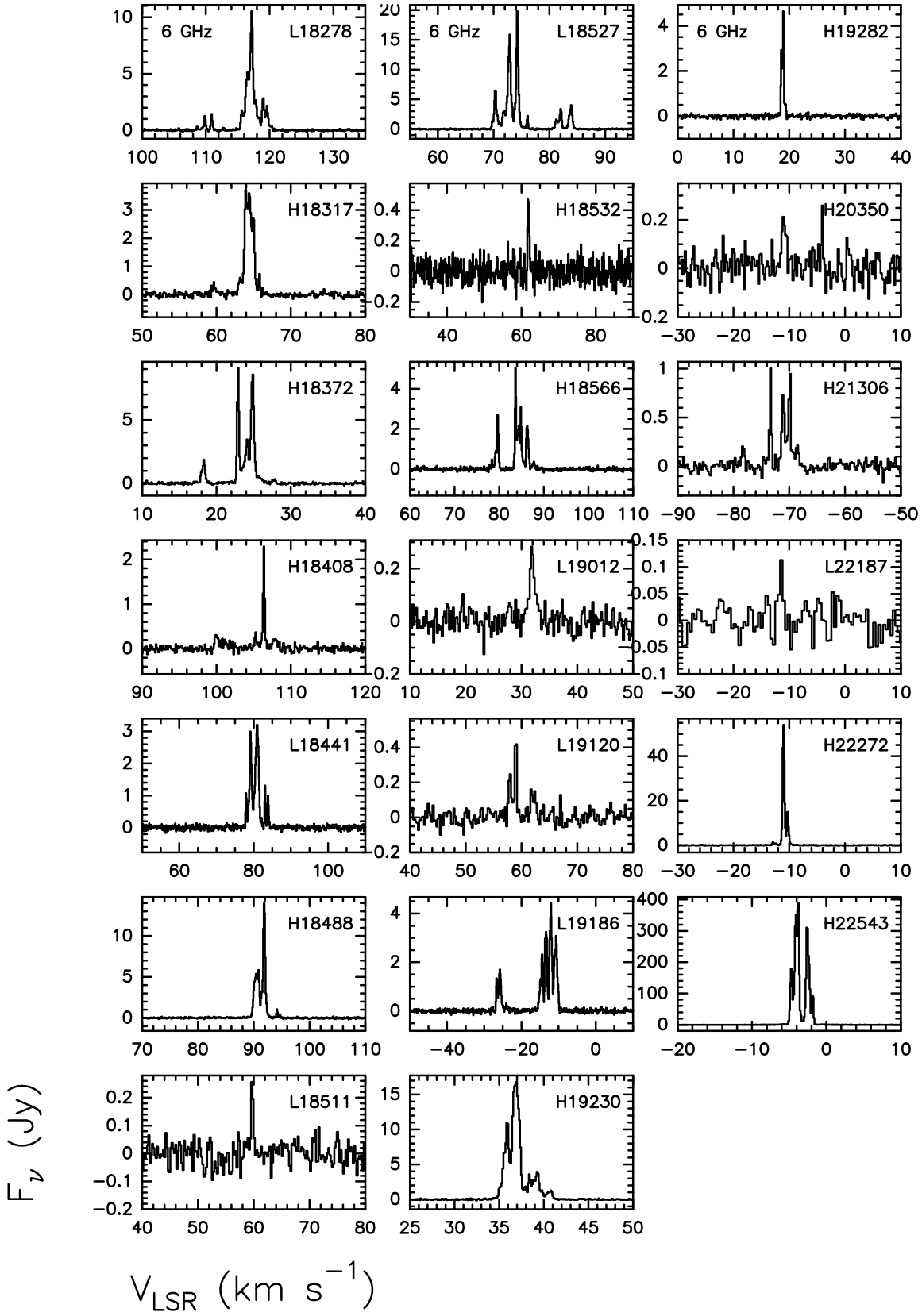

Fig. A.4. continued.

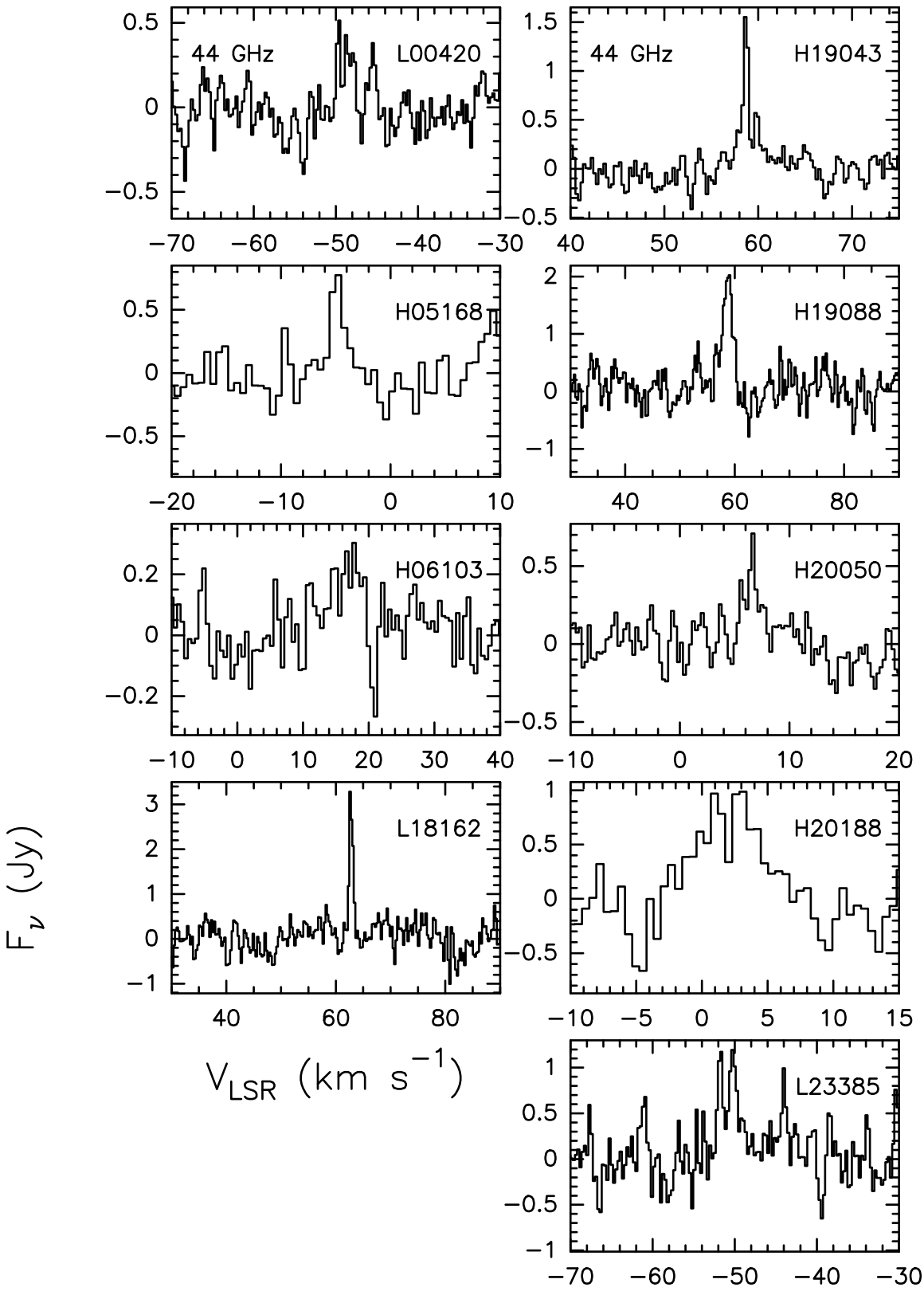

Fig. A.5. Same as Fig. A.1 for sources detected in the 44 GHz line only.

Appendix B: Tables

Table B.1. Source parameters used for the observations and detection summary.

IRAS name	type	RA (J2000)	Dec (J2000)	V_{LSR} km s^{-1}	CH_3OH 6 GHz	CH_3OH 44 GHz	CH_3OH 95 GHz	H_2O^p 22 GHz
00070+6503	L	00:09:43.7	+65:20:09	0.0	N	–	–	N
00117+6412	H	00:14:27.7	+64:28:46	–36.3	N	–	–	N
00127+6058[a]	L	00:15:29.1	+61:14:41	0.0	N	–	–	N^w
00338+6312[a]	H	00:36:47.5	+63:29:02	0.0	Y	–	–	N^v
00420+5530	L	00:44:57.6	+55:47:18	–51.2	N	*Y*	N	Y
00484+6531	L	00:51:33.0	+65:47:58	0.0	N	N	N	N
00554+6524	L	00:58:39.0	+65:40:42	0.0	N	N	N	N
01056+6251[a]	L	01:08:48.5	+63:07:19	0.0	N	–	–	N^w
01420+6401	L	01:45:39.6	+64:16:02	0.0	N	–	–	N
02383+6241	L	02:42:20.1	+62:53:51	0.0	N	N	N	N
02434+6018	L	02:47:15.8	+60:30:44	0.0	N	N	N	N
02593+6016[a]	H	03:03:17.9	+60:27:52	0.0	N	–	–	N^v
03064+5638	L	03:10:15.2	+56:50:18	0.0	N	N	N	N
03211+5446	L	03:24:59.1	+54:57:25	0.0	N	–	–	N
03353+5550	L	03:39:15.6	+55:59:48	0.0	N	N	N	N
03448+5545	L	03:48:47.9	+55:54:45	0.0	N	N	N	N
04000+5052	L	04:03:49.3	+51:00:48	0.0	N	N	N	N
04034+5116	H	04:07:11.9	+51:24:45	0.0	N	–	–	N
04156+5251[a]	L	04:19:32.7	+52:58:36	0.0	N	–	–	N^w
04269+3510[a]	L	04:30:14.4	+35:16:30	0.0	N	–	–	N^v
04579+4703	H	05:01:39.7	+47:07:23	–16.5	N	–	–	Y
05100+3723[a]	H	05:13:25.4	+37:27:04	0.0	N	–	–	N^w
05137+3919	L	05:17:13.3	+39:22:14	–25.4	*Y*	N	N	Y
05168+3634	H	05:20:16.1	+36:37:21	–15.1	N	*Y*^{m}	N	Y
05197+3355	L	05:23:04.4	+33:58:27	0.0	N	N	N	N
05236+3828	L	05:27:06.6	+38:31:18	0.0	N	N	N	N
05274+3345	H	05:30:45.6	+33:47:52	–3.8	Y	–	–	Y
05334+3149	H	05:36:41.1	+31:51:14	0.0	N	N	N	N
05345+3157	L	05:37:47.8	+31:59:24	–18.4	N	N	N	Y
05351+3549[a]	H	05:38:28.1	+35:51:15	0.0	N	–	–	N^w
05355+3039	L	05:38:47.2	+30:41:27	0.0	N	N	N	N
05358+3543[a]	H	05:39:10.4	+35:45:19	0.0	Y	–	–	Y^v
05373+2349	L	05:40:24.4	+23:50:54	2.3	N	N	N	Y
05382+3547	L	05:41:37.4	+35:48:49	0.0	N	–	–	N
05480+2545	H	05:51:10.6	+25:46:14	0.0	*Y*	*Y*	*Y*	N
05490+2658	H	05:52:12.8	+26:59:32	0.0	N	N	N	N
05553+1631	H	05:58:13.9	+16:32:00	6.1	N	N	N	Y
05554+2013	H	05:58:24.5	+20:13:57	0.0	N	N	N	N
05588+2625	L	06:01:55.2	+26:24:59	0.0	N	N	N	N
06001+3014[a]	L	06:03:22.9	+30:14:11	0.0	N	–	–	Y^v
06013+3030	L	06:04:34.2	+30:30:39	0.0	N	N	N	N
06055+2039[a]	H	06:08:32.8	+20:39:16	0.0	Y	–	–	Y^v
06056+2131	H	06:08:40.9	+21:31:01	2.6	Y	N	N	N
06058+2138[a]	H	06:08:54.1	+21:38:25	0.0	Y	–	–	Y^v
06061+2151	H	06:09:07.8	+21:50:39	–0.6	Y	N	N	Y
06063+2040	H	06:09:21.9	+20:39:28	0.0	N	–	–	N
06068+2030	L	06:09:51.7	+20:30:04	0.0	N	–	–	N
06084+1727[a]	H	06:11:24.5	+17:26:26	0.0	N	–	–	N^w
06099+1800[a]	L	06:12:53.3	+17:59:22	0.0	Y	–	–	Y^v
06103+1523	H	06:13:15.1	+15:22:36	15.6	N	*Y*^{m}	N	N
06104+1524	H	06:13:21.3	+15:23:57	0.0	N	–	–	N
06105+1756	H	06:13:28.3	+17:55:29	8.0	N	N	N	Y
06114+1745[a]	H	06:14:23.7	+17:44:36	0.0	N	–	–	N^v
06117+1350[a]	H	06:14:36.6	+13:49:35	0.0	Y	–	–	Y^v
06155+2319	H	06:18:35.2	+23:18:11	0.0	N	–	–	N
06158+1517[a]	L	06:18:44.8	+15:16:43	0.0	N	–	–	N^w
06291+0421	L	06:31:48.1	+04:19:31	0.0	N	–	–	Y
06299+1011	L	06:32:41.3	+10:09:34	0.0	N	–	–	N
06303+1021	L	06:33:04.4	+10:19:21	0.0	N	–	–	N
06308+0402	L	06:33:31.1	+04:00:07	0.0	N	–	–	N
06314+0427	L	06:34:05.5	+04:24:54	0.0	N	N	N	N
06382+0939	L	06:41:02.7	+09:36:10	5.2	N	N	N	N
06568-0411	L	06:59:22.4	–04:15:45	0.0	N	–	–	N

Table B.1. continued.

IRAS name	type	RA (J2000)	Dec (J2000)	V_{LSR} km s^{-1}	CH_3OH 6 GHz	CH_3OH 44 GHz	CH_3OH 95 GHz	H_2O^p 22 GHz
06584-0852	L	07:00:51.5	–08:56:29	41.3	N	N	N	Y
07029-1215[a]	L	07:05:16.9	–12:20:02	0.0	N	–	–	N[h]
07069-1045	H	07:09:20.5	–10:50:25	0.0	N	N	N	N
07284-1511[a]	H	07:30:42.5	–15:17:40	0.0	N	–	–	N[b]
07295-1915	L	07:31:47.6	–19:21:48	0.0	N	–	–	N
07333-1838[a]	H	07:35:34.3	–18:45:32	0.0	N	–	–	N[v]
07429-2523[a]	L	07:45:01.4	–25:31:10	0.0	N	–	–	N[w]
17417-2851	H	17:44:53.4	–28:52:20	–5.6	N	–	–	N
17450-2742	L	17:48:09.3	–27:43:21	–16.9	Y	–	–	N
17456-2850	H	17:48:47.1	–28:51:49	0.0	N	–	–	N
17495-2624	H	17:52:41.9	–26:25:32	17.3	N	–	–	N
17504-2519	H	17:53:35.1	–25:19:56	12.4	N	–	–	N
17527-2439	H	17:55:49.1	–24:40:20	13.2	N	N	N	Y
17571-2328	H	18:00:14.2	–23:28:57	0.0	*Y*	–	–	N
17580-2215	L	18:01:02.2	–22:15:45	0.0	N	–	–	N
17582-2234	L	18:01:18.0	–22:34:57	0.0	N	–	–	Y
17589-2312	H	18:01:57.1	–23:12:36	0.0	Y	–	–	N
18014-2428	L	18:04:29.6	–24:28:47	12.5	N	N	N	N
18018-2426	L	18:04:53.9	–24:26:41	10.5	N	Y	*Y*	N
18024-2119	L	18:05:25.4	–21:19:41	0.5	*Y*	*Y*	N	Y
18024-2231	L	18:05:30.6	–22:31:35	16.2	N	–	–	N
18026-2145	L	18:05:37.9	–21:45:06	0.0	N	–	–	N
18027-2202	H	18:05:46.2	–22:01:57	0.0	N	–	–	N
18039-2052	L	18:06:56.7	–20:51:51	0.0	N	–	–	N
18043-2153	L	18:07:23.2	–21:53:00	0.0	N	–	–	N
18048-2019	H	18:07:51.5	–20:18:36	49.1	Y	N	N	Y
18054-1818	L	18:08:24.0	–18:17:35	0.0	N	–	–	N
18078-1928	H	18:10:48.7	–19:27:42	0.0	N	–	–	N
18079-1756	H	18:10:50.3	–17:55:52	0.0	N	–	–	N
18081-2138	L	18:11:10.5	–21:38:15	0.0	N	–	–	N
18089-1732	H	18:11:51.3	–17:31:29	32.9	Y	Y	*Y*	Y
18102-1800	H	18:13:12.1	–17:59:34	0.0	Y	–	–	N
18115-1701	L	18:14:25.6	–17:00:53	0.0	N	–	–	N
18122-1751	L	18:15:12.2	–17:49:60	0.0	N	–	–	N
18123-1203	L	18:15:07.3	–12:02:42	0.0	N	–	–	N
18131-1606	L	18:16:01.9	–16:05:05	0.0	N	–	–	N
18132-1638	L	18:16:08.8	–16:37:07	0.0	N	–	–	N
18134-1942	H	18:16:22.2	–19:41:20	10.5	Y	N	N	Y
18136-1347	L	18:16:28.6	–13:46:33	0.0	N	–	–	N
18144-1723	L	18:17:24.4	–17:22:13	47.3	Y	Y	*Y*	Y
18145-1557	H	18:17:26.7	–15:56:19	0.0	N	–	–	N
18151-1208	H	18:17:57.1	–12:07:22	32.8	Y	Y	N	N
18153-1651	H	18:18:15.9	–16:50:37	0.0	N	–	–	N
18156-1343	L	18:18:28.6	–13:42:22	0.0	N	–	–	N
18159-1550	H	18:18:47.6	–15:48:54	59.7	N	–	–	N
18159-1648	H	18:18:53.0	–16:47:39	22.1	Y	Y	*Y*	N
18160-1641	L	18:18:57.3	–16:40:15	0.0	N	–	–	N
18162-1612	L	18:19:07.5	–16:11:21	61.8	N	Y	N	N
18167-1614	L	18:19:37.7	–16:13:11	0.0	N	–	–	N
18171-1548	H	18:20:04.6	–15:46:47	0.0	N	–	–	N
18181-1534	L	18:20:58.9	–15:33:10	0.0	Y	–	–	N
18195-1407	L	18:22:24.4	–14:05:33	0.0	N	–	–	N
18197-1351	H	18:22:36.7	–13:50:11	0.0	N	–	–	N
18198-1429	H	18:22:41.7	–14:27:35	0.0	N	–	–	N
18212-1320	H	18:24:04.7	–13:19:16	0.0	N	–	–	N
18224-1228	L	18:25:12.6	–12:27:09	0.0	Y	–	–	N
18230-1248	L	18:25:51.7	–12:46:15	0.0	N	–	–	N
18236-1205	H	18:26:24.3	–12:03:47	26.2	Y	–	–	Y
18247-1147	H	18:27:31.1	–11:45:56	55.9	*Y*	–	–	N
18248-1218	L	18:27:37.9	–12:16:27	0.0	N	–	–	N
18256-0742	L	18:28:20.5	–07:40:22	36.7	N	N	N	N
18258-0737	H	18:28:34.1	–07:35:31	37.9	N	–	–	N
18265-1517	H	18:29:24.8	–15:15:49	0.0	Y	–	–	N
18278-1009	L	18:30:35.2	–10:07:12	93.7	Y	N	N	N
18288-0158	L	18:31:26.6	–01:56:35	5.8	N	N	N	N

Table B.1. continued.

IRAS name	type	RA (J2000)	Dec (J2000)	V_{LSR} km s^{-1}	CH_3OH 6 GHz	CH_3OH 44 GHz	CH_3OH 95 GHz	H_2O^p 22 GHz
18310-0825	H	18:33:47.2	–08:23:34	0.0	N	–	–	N
18311-0701	L	18:33:52.8	–06:58:44	0.0	N	–	–	N
18314-0820	H	18:34:08.9	–08:17:52	0.0	N	–	–	N
18314-0517	L	18:34:05.9	–05:14:49	0.0	N	–	–	N
18316-0602	H	18:34:19.8	–05:59:44	42.2	Y	*Y*	*Y*^{m}	Y
18317-0845	H	18:34:29.9	–08:43:22	0.0	Y	–	–	N
18317-0513	H	18:34:25.9	–05:10:59	42.2	N	–	–	N
18318-0741	L	18:34:30.8	–07:38:54	0.0	N	–	–	N
18355-0550	L	18:38:13.6	–05:48:17	0.0	N	–	–	N
18358-0647	H	18:38:31.3	–06:44:29	0.0	N	–	–	N
18360-0537	H	18:38:40.3	–05:35:06	102.3	N	*Y*	*Y*	Y
18363-0554	L	18:39:03.7	–05:52:15	65.2	N	N	N	N
18372-0541	H	18:39:56.0	–05:38:49	22.8	Y	–	–	N
18396-0431	L	18:42:18.8	–04:28:37	97.3	N	*Y*^{m}	*Y*	N
18408-0353	H	18:43:28.8	–03:50:20	0.0	*Y*	–	–	N
18408-0348	H	18:43:31.1	–03:44:57	0.0	N	–	–	N
18411-0312	L	18:43:46.4	–03:09:54	0.0	N	–	–	N
18424-0329	L	18:45:03.3	–03:26:49	47.9	N	N	N	N
18441-0134	L	18:46:44.2	–01:30:55	0.0	Y	–	–	N
18445-0222	H	18:47:10.7	–02:19:06	86.9	N	–	–	N
18463-0052	L	18:48:52.8	–00:49:02	0.0	N	–	–	N
18488+0000	H	18:51:24.8	+00:04:19	83.2	Y	–	–	N
18507+0121	H	18:53:17.4	+01:24:55	57.1	Y	*Y*	N	Y
18511+0146	L	18:53:38.1	+01:50:27	56.8	*Y*	–	–	N
18517+0437	H	18:54:13.8	+04:41:32	43.7	Y	*Y*	N	Y
18527+0301	L	18:55:16.5	+03:05:07	76.0	Y	N	N	N
18532+0047	H	18:55:50.8	+00:51:22	58.6	*Y*	–	–	N
18537+0145	L	18:56:15.0	+01:49:03	0.0	N	–	–	N
18544+0112	L	18:56:59.8	+01:16:20	0.0	N	–	–	N
18551+0302	H	18:57:42.1	+03:06:04	57.5	N	–	–	N
18565+0349	L	18:59:03.4	+03:53:22	91.6	N	N	N	N
18566+0408	H	18:59:09.8	+04:12:14	85.1	Y	–	–	N
18567+0700	L	18:59:13.6	+07:04:47	29.4	N	N	N	N
18571+0326	L	18:59:40.2	+03:30:29	0.0	N	–	–	N
18571+0349	L	18:59:40.1	+03:53:35	56.2	N	–	–	N
18586+0106	L	19:01:10.6	+01:11:16	37.9	N	N	N	N
18596+0536	H	19:02:06.5	+05:40:33	0.0	N	–	–	N
19001+0402	H	19:02:36.2	+04:06:58	50.7	N	–	–	N
19002+0454	H	19:02:42.0	+04:58:49	69.2	N	–	–	N
19012+0505	L	19:03:43.5	+05:09:49	40.4	Y	–	–	N
19023+0538	L	19:04:49.0	+05:42:40	0.0	N	–	–	N
19043+0726	H	19:06:47.6	+07:31:38	58.9	N	*Y*	N	N
19045+0518	H	19:06:59.3	+05:22:57	53.6	N	–	–	N
19045+0813	H	19:06:59.8	+08:18:43	0.0	N	–	–	Y
19077+0839	L	19:10:09.6	+08:44:11	0.0	N	–	–	N
19088+0902	H	19:11:15.9	+09:07:27	59.6	N	*Y*	N	Y
19092+0841	L	19:11:37.4	+08:46:30	58.0	Y	Y	N	Y
19094+0944	H	19:11:52.0	+09:49:46	65.3	N	–	–	N
19118+0945	L	19:14:14.7	+09:50:40	0.0	N	–	–	N
19120+1148	L	19:14:22.1	+11:53:39	0.0	*Y*	–	–	N
19124+1106	H	19:14:45.3	+11:11:57	0.0	N	–	–	N
19139+1137	L	19:16:18.7	+11:42:46	0.0	N	–	–	N
19183+1556	L	19:20:37.6	+16:02:31	0.0	N	–	–	N
19186+1440	L	19:20:56.9	+14:46:40	0.0	Y	–	–	N
19198+1423	H	19:22:07.7	+14:29:20	58.9	N	–	–	N
19202+1412	L	19:22:31.5	+14:18:30	0.0	N	–	–	N
19213+1723	H	19:23:37.0	+17:28:59	41.7	N	N	N	Y
19214+1458	H	19:23:46.1	+15:04:51	0.0	N	–	–	N
19230+1341	H	19:25:22.1	+13:47:19	0.0	Y	–	–	N
19282+1814	H	19:30:28.1	+18:20:53	24.1	Y	N	N	N
19282+1742	H	19:30:30.4	+17:48:30	0.0	N	–	–	N
19294+1649	L	19:31:44.8	+16:55:57	0.0	N	–	–	N
19295+1637	L	19:31:50.9	+16:43:29	0.0	N	–	–	N
19325+1925	H	19:34:45.9	+19:31:41	0.0	N	–	–	N
19332+2028	L	19:35:25.4	+20:34:56	0.0	N	–	–	N

Table B.1. continued.

IRAS name	type	RA (J2000)	Dec (J2000)	V_{LSR} km s^{-1}	CH_3OH 6 GHz	CH_3OH 44 GHz	CH_3OH 95 GHz	H_2O^p 22 GHz
19343+2026	L	19:36:30.2	+20:33:08	0.0	N	–	–	N
19368+2239	H	19:38:58.1	+22:46:32	36.4	N	–	–	N
19374+2352	H	19:39:33.2	+23:59:55	36.9	N	N	N	Y
19383+2711	H	19:40:22.1	+27:18:34	0.0	N	–	–	N
19388+2357	H	19:40:59.3	+24:04:39	34.6	Y	*Y*	N	Y
19423+2541	H	19:44:23.4	+25:48:40	0.0	N	–	–	N
19458+2442	L	19:47:59.7	+24:50:19	0.0	N	–	–	N
19462+2759	H	19:48:14.0	+28:07:23	0.0	N	–	–	N
19499+2613	H	19:52:01.4	+26:21:10	0.0	N	–	–	N
19542+3004	L	19:56:13.2	+30:12:56	0.0	N	–	–	N
19560+3135	H	19:58:03.3	+31:44:06	0.0	N	–	–	N
19592+3302	H	20:01:09.8	+33:11:08	0.0	N	–	–	N
20028+2903	L	20:04:53.3	+29:11:37	0.0	N	–	–	N
20050+2720	H	20:07:06.7	+27:28:53	6.4	N	*Y*	N	Y
20051+3435	H	20:07:03.8	+34:44:34	0.0	N	–	–	N
20056+3350	H	20:07:31.5	+33:59:39	9.4	N	N	N	Y
20062+3550	H	20:08:09.7	+35:59:20	0.6	Y	*Y*	N	Y
20081+2720	H	20:10:11.4	+27:29:06	0.0	N	–	–	N
20099+3640	L	20:11:46.4	+36:49:37	–36.4	N	N	N	N
20103+3633	H	20:12:13.9	+36:42:58	0.0	N	–	–	N
20106+3545	L	20:12:31.3	+35:54:46	7.8	N	N	N	N
20126+4104	H	20:14:26.0	+41:13:32	–3.9	Y	Y	*Y*	Y
20149+3440	L	20:16:50.4	+34:49:22	0.0	N	–	–	N
20153+3850[a]	L	20:17:07.6	+38:59:25	0.0	N	–	–	N[b]
20160+3636[a]	H	20:17:56.1	+36:45:33	0.0	N	–	–	N[b]
20173+3714	L	20:19:10.4	+37:23:31	0.0	N	–	–	N
20180+3558	L	20:19:58.0	+36:07:37	0.0	N	–	–	N
20188+3928	H	20:20:39.3	+39:37:52	1.5	N	*Y*	N	Y
20190+4102	L	20:20:47.9	+41:12:08	0.0	N	–	–	N
20205+3948	H	20:22:21.8	+39:58:04	0.0	N	–	–	N
20216+4107	H	20:23:23.8	+41:17:40	0.0	N	–	–	N
20217+3947	L	20:23:31.7	+39:57:23	–0.9	N	N	N	N
20220+3728	H	20:23:55.6	+37:38:10	–2.7	N	–	–	N
20222+3541	L	20:24:10.9	+35:51:37	0.0	N	–	–	N
20227+4154	H	20:24:31.4	+42:04:17	5.9	N	N	N	Y
20228+4215[a]	L	20:24:34.4	+42:25:01	0.0	N	–	–	N[b]
20243+3853	H	20:26:10.8	+39:03:29	0.0	N	–	–	N
20261+3825	L	20:28:01.9	+38:35:50	0.0	N	–	–	N
20264+4042	H	20:28:12.3	+40:52:28	0.0	N	–	–	N
20277+3851	H	20:29:36.7	+39:01:17	0.0	N	–	–	N
20278+3521	L	20:29:46.9	+35:31:39	–4.5	N	N	N	N
20281+4038	H	20:29:54.7	+40:48:52	0.0	N	–	–	N
20286+4105	H	20:30:27.9	+41:15:48	–3.8	N	–	–	Y
20293+4007	L	20:31:07.9	+40:17:23	0.0	N	–	–	N
20306+4005	H	20:32:28.7	+40:16:05	0.0	N	–	–	N
20306+3749	H	20:32:34.4	+37:59:35	0.0	N	–	–	N
20319+3958	H	20:33:49.4	+40:08:44	0.0	N	–	–	N
20321+4112	H	20:33:55.6	+41:22:43	0.0	N	–	–	N
20327+4120	L	20:34:31.1	+41:30:44	0.0	N	–	–	N
20332+4124	H	20:35:00.5	+41:34:48	0.0	N	–	–	N
20333+4102	L	20:35:09.5	+41:13:18	8.4	N	–	–	N
20337+4104	L	20:35:34.7	+41:15:21	0.0	N	–	–	N
20343+4129	H	20:36:07.1	+41:40:01	0.0	N	–	–	N
20350+4126	H	20:36:52.5	+41:36:33	0.0	Y	–	–	N
20406+4555	L	20:42:21.6	+46:05:53	0.0	N	–	–	N
20444+4629	H	20:46:08.2	+46:40:41	–4.1	N	N	N	N
20446+4613	L	20:46:17.3	+46:24:38	0.0	N	–	–	N
21020+4939[a]	L	21:03:42.2	+49:51:53	0.0	N	–	–	N[w]
21036+4927[a]	H	21:05:15.6	+49:40:01	0.0	N	–	–	N[w]
21046+5110	L	21:06:16.3	+51:22:13	0.0	N	–	–	N
21078+5211	H	21:09:25.2	+52:23:44	–6.1	N	N	N	Y
21080+4758	L	21:09:46.5	+48:10:59	0.0	N	–	–	N
21202+5157	H	21:21:53.2	+52:10:44	0.0	N	–	–	N
21270+5423[a]	L	21:28:42.0	+54:36:51	0.0	N	–	–	N[w]
21306+5540[a]	H	21:32:11.6	+55:53:24	0.0	*Y*	–	–	Y[v]

Table B.1. continued.

IRAS name	type	RA (J2000)	Dec (J2000)	V_{LSR} km s^{-1}	CH_3OH 6 GHz	CH_3OH 44 GHz	CH_3OH 95 GHz	H_2O^p 22 GHz
21307+5049	L	21:32:31.5	+51:02:22	–46.7	N	N	N	Y
21336+5333	H	21:35:21.0	+53:47:12	0.0	N	–	–	N
21391+5802	H	21:40:42.3	+58:16:10	0.4	N	Y	Y	Y
21418+6552[a]	H	21:43:02.3	+66:06:29	0.0	N	–	–	Y[v]
21418+5403[a]	H	21:43:29.8	+54:16:56	0.0	N	–	–	N[w]
21519+5613	H	21:53:39.2	+56:27:46	–63.2	N	–	–	N
21526+5728	H	21:54:18.4	+57:42:51	0.0	N	–	–	N
21548+5747	L	21:56:29.9	+58:01:35	0.0	N	–	–	N
22147+5948	L	22:16:28.6	+60:03:49	0.0	N	–	–	N
22172+5549	L	22:19:09.0	+56:04:45	–43.8	N	N	N	N
22187+5559	L	22:20:34.9	+56:14:40	0.0	*Y*	–	–	N
22198+6336	H	22:21:27.6	+63:51:42	–11.1	N	N	N	Y
22267+6244	H	22:28:29.3	+62:59:44	–1.5	N	N	N	N
22272+6358	H	22:28:52.2	+64:13:43	–9.9	Y	N	N	N
22305+5803	H	22:32:24.3	+58:18:58	–52.1	N	–	–	Y
22344+5909	L	22:36:20.6	+59:24:57	0.0	N	–	–	N
22457+5751	L	22:47:46.5	+58:07:19	0.0	N	–	–	N
22475+5939[a]	H	22:49:29.5	+59:54:57	0.0	N	–	–	Y[v]
22506+5944	H	22:52:38.6	+60:00:56	–51.5	*Y*	*Y*	*Y*[m]	Y
22539+5758[a]	H	22:56:00.0	+58:14:46	0.0	N	–	–	N[v]
22542+5815[a]	L	22:56:17.0	+58:31:13	0.0	N	–	–	N[v]
22543+6145[a]	H	22:56:19.1	+62:01:57	0.0	Y	–	–	Y[v]
22551+6221	H	22:57:05.2	+62:37:44	0.0	N	–	–	N
22566+5830[a]	H	22:58:41.3	+58:46:57	0.0	N	–	–	Y[v]
22570+5912	H	22:59:06.4	+59:28:28	0.0	N	–	–	N
23026+5948	L	23:04:45.7	+60:04:35	–51.1	N	N	N	N
23042+6000	L	23:06:21.2	+60:16:16	0.0	N	N	N	N
23134+6131	L	23:15:34.5	+61:47:41	0.0	N	N	N	N
23140+6121	L	23:16:11.7	+61:37:45	–51.5	N	N	N	N
23146+5954	L	23:16:48.9	+60:10:46	0.0	N	–	–	N
23152+6034	L	23:17:25.8	+60:50:45	0.0	N	–	–	N
23314+6033	L	23:33:44.4	+60:50:30	–45.4	N	N	N	N
23330+6437	L	23:35:23.7	+64:54:31	0.0	N	–	–	N
23385+6053	L	23:40:53.2	+61:10:21	–50.0	N	Y	N	Y
23448+6010	L	23:47:20.2	+60:27:21	0.0	N	–	–	N
23504+6012[a]	L	23:52:58.2	+60:28:45	0.0	N	–	–	N[w]
23507+6230	L	23:53:12.9	+62:47:00	0.0	N	–	–	N
23545+6508	H	23:57:05.2	+65:25:11	–18.4	N	–	–	N

Notes. The new detections are in italics. [(p)] Observed by Palla et al. (1991) with the Medicina 32-m telescope, except when differently specified. [(a)] Rejected by Palla et al. (1991) because associated with radio continuum. [(w)] Observed by Wouterloot et al. (1993). [(v)] Observed by Valdettaro et al. (2001). [(m)] Marginal detection at $\sim 3\sigma$. [(h)] Observed by Henning et al. (1992). [(b)] Observed with the Medicina 32-m telescope (unpublished data).

Table B.2. Parameters of the 6 GHz CH_3OH maser (Class II) detected in *high* sources with the Effelsberg 100-m telescope.

Source	V_{LSR}[a] (km s^{-1})	$\int F_\nu dV$ (Jy km s^{-1})	V (km s^{-1})	ΔV (km s^{-1})	F_{peak} (Jy)
00338+6312*	−17.5[f]	6.4 ± 0.1	−23.030 ± 0.001	0.287 ± 0.003	21.0
		2.8 ± 0.2	−22.64 ± 0.02	0.74 ± 0.04	3.62
05274+3345	–3.8	2.40 ± 0.04	0.324 ± 0.002	0.331 ± 0.006	6.81
		10.07 ± 0.04	1.244 ± 0.003	0.584 ± 0.004	16.2
		16.59 ± 0.04	1.609 ± 0.0005	0.349 ± 0.003	44.6
		1.15 ± 0.03	2.140 ± 0.003	0.202 ± 0.005	5.35
05358+3543*	−17.6[d]	18 ± 1	−13.8 ± 0.1	0.5 ± 0.1	34.4
		15 ± 1	−13.2 ± 0.1	0.3 ± 0.1	45.7
		19 ± 1	−12.8 ± 0.1	0.3 ± 0.1	51.8
		1.5 ± 1	−11.5 ± 0.1	3.0 ± 0.1	0.47
05480+2545	–9.3[b]	0.98 ± 0.03	−15.250 ± 0.004	0.238 ± 0.009	3.88
		3.09 ± 0.04	−14.730 ± 0.003	0.426 ± 0.007	6.81
		0.27 ± 0.03	−13.99 ± 0.02	0.30 ± 0.05	0.84
		6.15 ± 0.04	−4.8940 ± 0.0001	0.340 ± 0.003	17.0
06055+2039*	8.8[c]	0.2 ± 0.02	3.9 ± 0.02	0.38 ± 0.06	0.5
		0.78 ± 0.02	5.496 ± 0.006	0.47 ± 0.02	1.57
06056+2131	2.6	3.7 ± 0.2	8.8 ± 0.1	0.3 ± 0.1	12.7
		2.2 ± 0.2	9.6 ± 0.1	0.3 ± 0.1	7.26
		0.7 ± 0.2	10.6 ± 0.1	1.1 ± 0.1	0.605
06058+2138*	3.1[c]	4.1 ± 0.2	8.470 ± 0.009	0.43 ± 0.03	9.10
		5.0 ± 0.1	9.446 ± 0.001	0.386 ± 0.008	12.2
		373.0 ± 0.2	10.590 ± 0.001	0.784 ± 0.001	447
		17.7 ± 0.1	11.45 ± 0.01	0.212 ± 0.002	78.7
06061+2151	–0.6	0.51 ± 0.02	−5.564 ± 0.003	0.232 ± 0.008	2.08
		0.17 ± 0.03	−5.05 ± 0.06	0.7 ± 0.2	0.227
		0.30 ± 0.02	10.63 ± 0.03	0.74 ± 0.07	0.380
06117+1350*	17.9[c]	2.2 ± 0.8	14.6 ± 0.1	0.2 ± 0.1	9.5
		25.0 ± 0.8	15.1 ± 0.1	0.5 ± 0.1	47.8
		4.6 ± 0.8	15.7 ± 0.1	0.5 ± 0.1	8.2
17571-2328	–	0.85 ± 0.01	143.80 ± 0.03	1.16 ± 0.05	0.686
		0.29 ± 0.03	147.30 ± 0.02	0.37 ± 0.05	0.731
17589-2312	21.1[c]	1.5 ± 0.5	13.1 ± 0.1	1.0 ± 0.1	1.44
		7.1 ± 0.5	14.7 ± 0.1	0.4 ± 0.1	19.1
		9.6 ± 0.5	15.2 ± 0.1	0.2 ± 0.1	39.3
		54.7 ± 0.5	16.0 ± 0.1	0.8 ± 0.1	62.5
		2.21 ± 0.06	17.430 ± 0.006	0.48 ± 0.02	4.30
		2.59 ± 0.04	18.7000 ± 0.0008	0.239 ± 0.005	10.2
		3.80 ± 0.05	19.540 ± 0.003	0.436 ± 0.008	8.19
		1.08 ± 0.07	24.60 ± 0.04	1.19 ± 0.06	0.847
		15.60 ± 0.07	25.4500 ± 0.0008	0.569 ± 0.002	25.8
		26.07 ± 0.05	26.4800 ± 0.0009	0.937 ± 0.002	26.1
		10.0 ± 0.4	28.07 ± 0.02	1.27 ± 0.04	7.37
		7.8 ± 0.2	28.630 ± 0.003	0.422 ± 0.007	17.2
18048-2019	49.1	15.3 ± 0.6	41.40 ± 0.110	0.6142 ± 0.110	23.3
		17.7 ± 0.6	42.1 ± 0.1	0.6 ± 0.1	27.3
		5.9 ± 0.6	43.2 ± 0.1	0.4 ± 0.1	15.5
		0.7 ± 0.6	44.2 ± 0.1	1.0 ± 0.1	0.629
		4.1 ± 0.4	45.8 ± 0.1	1.9 ± 0.1	2.03
		5.6 ± 0.4	46.8 ± 0.1	0.8 ± 0.1	6.67
		5.2 ± 0.4	47.1 ± 0.1	0.3 ± 0.1	14.6
		1.4 ± 0.4	48.1 ± 0.1	0.7 ± 0.1	1.82
		1.0 ± 0.4	50.4 ± 0.1	1.0 ± 0.1	1.00
18089-1732	32.9	2.8 ± 0.1	29.59 ± 0.08	3.4 ± 0.2	0.774
		0.13 ± 0.01	29.210 ± 0.004	0.111 ± 0.003	1.07
		0.94 ± 0.03	30.210 ± 0.003	0.270 ± 0.009	3.26
		3.3 ± 0.7	31.9 ± 0.1	0.7 ± 0.1	4.50
		4.7 ± 0.7	32.8 ± 0.1	0.5 ± 0.1	9.18
		24.7 ± 0.7	33.7 ± 0.1	0.5 ± 0.1	50.3
		3.8 ± 0.7	34.7 ± 0.1	0.4 ± 0.1	8.22
		1.9 ± 0.7	36.5 ± 0.1	0.5 ± 0.1	3.87
	32.9	5.3 ± 0.7	37.9 ± 0.1	1.1 ± 0.1	4.61
		5.8 ± 0.7	38.7 ± 0.1	0.3 ± 0.1	17.2
		27.1 ± 0.7	39.2 ± 0.1	0.5 ± 0.1	55.4
		3.6 ± 0.7	42.4 ± 0.1	10.4 ± 0.1	0.321

Table B.2. continued.

Source	V_{LSR}[a] (km s^{-1})	$\int F_\nu dV$ (Jy km s^{-1})	V (km s^{-1})	ΔV (km s^{-1})	F_{peak} (Jy)
18102-1800	21.1[d]	3.8 ± 0.1	21.6 ± 0.1	0.5 ± 0.1	7.05
		1.5 ± 0.1	23.1 ± 0.1	0.4 ± 0.1	3.09
		2.9 ± 0.1	24.0 ± 0.1	0.6 ± 0.1	4.23
		1.40 ± 0.04	25.020 ± 0.006	0.49 ± 0.02	2.69
		1.11 ± 0.04	25.640 ± 0.007	0.46 ± 0.02	2.28
		0.19 ± 0.03	27.22 ± 0.03	0.51 ± 0.1	0.35
18134-1942	10.5	2.28 ± 0.08	4.877 ± 0.004	0.28 ± 0.01	7.56
		42 ± 3	6.4 ± 0.1	1.1 ± 0.1	35.0
		37 ± 3	6.6 ± 0.1	0.3 ± 0.1	107.
		40 ± 3	7.7 ± 0.1	0.4 ± 0.1	83.2
		8 ± 3	8.3 ± 0.1	0.5 ± 0.1	16.7
		14 ± 3	8.8 ± 0.1	0.4 ± 0.1	31.1
		3 ± 3	13.3 ± 0.1	0.5 ± 0.1	5.64
		1.6 ± 0.3	14.4 ± 0.1	0.5 ± 0.1	3.01
		7.3 ± 0.4	14.7 ± 0.1	0.4 ± 0.1	16.4
		2.5 ± 0.4	15.4 ± 0.1	0.4 ± 0.1	5.26
		1.3 ± 0.4	16.1 ± 0.1	0.4 ± 0.1	3.20
18151-1208	32.8	11.75 ± 0.09	27.630 ± 0.002	0.323 ± 0.003	34.1
		31.16 ± 0.08	28.000 ± 0.003	0.258 ± 0.007	113.
		0.57 ± 0.05	28.990 ± 0.007	0.30 ± 0.03	1.78
18159-1648	22.1	0.20 ± 0.04	22.7 ± 0.1	1.2 ± 0.4	0.154
18236-1205	26.2	0.9 ± 0.2	25.1 ± 0.1	1.1 ± 0.1	0.746
		1.8 ± 0.2	25.2 ± 0.1	0.5 ± 0.1	3.37
		3.6 ± 0.2	27.2 ± 0.1	0.5 ± 0.1	6.19
		3.0 ± 0.2	28.7 ± 0.1	0.5 ± 0.1	5.98
		0.3 ± 0.2	29.9 ± 0.1	0.9 ± 0.1	0.341
18247-1147	55.9	0.34 ± 0.02	116.300 ± 0.005	0.23 ± 0.01	1.38
		0.31 ± 0.02	123.00 ± 0.02	0.39 ± 0.04	0.756
18265-1517	19.0[b]	8.83 ± 0.06	14.900 ± 0.003	0.256 ± 0.002	32.4
		1.44 ± 0.09	15.55 ± 0.02	0.53 ± 0.04	2.55
		6.02 ± 0.06	17.250 ± 0.002	0.324 ± 0.004	17.4
		2.33 ± 0.06	18.660 ± 0.005	0.38 ± 0.01	5.82
18316-0602	42.2	0.5 ± 0.4	38.5 ± 0.1	0.4 ± 0.1	1.41
		4.0 ± 0.4	41.0 ± 0.1	0.9 ± 0.1	4.04
		39.3 ± 0.4	41.8 ± 0.1	0.3 ± 0.1	118.
		0.7 ± 0.4	42.5 ± 0.1	0.4 ± 0.1	1.87
18317-0845	62.4	0.22 ± 0.03	59.67 ± 0.05	0.7 ± 0.1	0.304
		0.27 ± 0.04	63.15 ± 0.03	0.48 ± 0.06	0.537
		0.60 ± 0.07	63.890 ± 0.005	0.28 ± 0.02	1.99
		3.5 ± 0.1	64.39 ± 0.01	0.96 ± 0.04	3.39
		0.49 ± 0.05	65.020 ± 0.005	0.26 ± 0.02	1.75
		0.18 ± 0.02	65.77 ± 0.01	0.22 ± 0.02	0.771
18372-0541	22.8	0.95 ± 0.04	18.25 ± 0.01	0.54 ± 0.02	1.65
		2.81 ± 0.03	22.900 ± 0.001	0.296 ± 0.004	8.91
		2.8 ± 0.1	24.06 ± 0.02	1.00 ± 0.06	2.67
		3.7 ± 0.1	24.860 ± 0.003	0.433 ± 0.007	8.11
18408-0353	102.1[b]	0.20 ± 0.04	100.00 ± 0.06	0.7 ± 0.2	0.293
		0.11 ± 0.03	105.30 ± 0.03	0.3 ± 0.1	0.334
		0.57 ± 0.02	106.400 ± 0.003	0.238 ± 0.009	2.24
18488+0000	83.2	2.7 ± 0.3	90.2 ± 0.1	0.6 ± 0.1	4.17
		1.7 ± 0.3	90.9 ± 0.1	0.4 ± 0.1	3.78
		0.6 ± 0.3	91.4 ± 0.1	0.2 ± 0.1	2.69
		6.3 ± 0.3	91.9 ± 0.1	0.4 ± 0.1	13.8
		0.27 ± 0.02	94.190 ± 0.007	0.24 ± 0.02	1.07
		0.12 ± 0.02	94.69 ± 0.02	0.25 ± 0.04	0.478

Table B.2. continued.

Source	V_{LSR}[a] (km s^{-1})	$\int F_\nu dV$ (Jy km s^{-1})	V (km s^{-1})	ΔV (km s^{-1})	F_{peak} (Jy)
18507+0121	57.1	8.62 ± 0.02	55.660 ± 0.003	0.394 ± 0.003	20.6
		0.17 ± 0.01	57.860 ± 0.003	0.20 ± 0.01	0.766
		0.93 ± 0.08	59.9 ± 0.1	0.4 ± 0.1	2.05
		1.8 ± 0.08	62.5 ± 0.1	0.6 ± 0.1	2.73
18517+0437	43.7	1.4 ± 0.1	39.64 ± 0.03	1.0 ± 0.1	1.33
		138.1 ± 0.3	41.180 ± 0.003	0.524 ± 0.003	248.
		1.56 ± 0.2	42.75 ± 0.04	0.8 ± 0.1	1.88
		3.2 ± 0.2	45.34 ± 0.05	1.7 ± 0.1	1.81
		1.67 ± 0.08	45.910 ± 0.004	0.23 ± 0.01	6.74
		0.69 ± 0.08	48.22 ± 0.02	0.40 ± 0.06	1.62
		2.35 ± 0.08	51.26 ± 0.01	0.50 ± 0.02	4.38
18532+0047	58.6	0.23 ± 0.02	61.89 ± 0.02	0.48 ± 0.05	0.449
18566+0408	85.1	0.12 ± 0.02	78.41 ± 0.02	0.26 ± 0.05	0.447
		0.31 ± 0.02	79.19 ± 0.01	0.33 ± 0.03	0.882
		1.12 ± 0.02	79.680 ± 0.004	0.37 ± 0.01	2.80
		1.56 ± 0.07	83.7 ± 0.1	0.3 ± 0.1	4.72
		1.39 ± 0.07	84.3 ± 0.1	0.6 ± 0.1	2.09
		0.96 ± 0.07	84.9 ± 0.1	0.3 ± 0.1	2.65
		1.31 ± 0.07	86.3 ± 0.1	0.6 ± 0.1	2.18
		0.23 ± 0.07	87.7 ± 0.1	0.7 ± 0.1	0.302
19230+1341	39.6	6.69 ± 0.01	35.800 ± 0.001	0.658 ± 0.003	9.56
		16.10 ± 0.05	36.900 ± 0.001	0.867 ± 0.003	17.4
		1.00 ± 0.03	38.390 ± 0.003	0.32 ± 0.01	2.97
		3.43 ± 0.05	39.180 ± 0.005	0.93 ± 0.02	3.47
		0.95 ± 0.03	40.65 ± 0.01	0.74 ± 0.03	1.20
19282+1814	24.1	1.55 ± 0.02	18.860 ± 0.004	0.513 ± 0.008	2.83
19388+2357	34.6	3.3 ± 0.4	36.4 ± 0.1	0.7 ± 0.1	4.18
		3.5 ± 0.4	37.2 ± 0.1	0.5 ± 0.1	6.75
		8.8 ± 0.4	38.2 ± 0.1	0.4 ± 0.1	23.0
		0.4 ± 0.4	38.7 ± 0.1	0.2 ± 0.1	1.63
		1.1 ± 0.4	39.6 ± 0.1	0.4 ± 0.1	2.90
20062+3550	0.6	0.49 ± 0.05	−3.0 ± 0.1	0.5 ± 0.1	0.883
		0.48 ± 0.05	−2.6 ± 0.1	0.3 ± 0.1	1.57
		1.47 ± 0.05	5.9 ± 0.1	0.4 ± 0.1	3.75
	0.6	0.83 ± 0.05	6.6 ± 0.1	0.4 ± 0.1	1.92
20126+4104	–3.9	1.49 ± 0.03	−8.393 ± 0.005	0.56 ± 0.02	2.52
		4.6 ± 0.9	−7.7 ± 0.1	0.4 ± 0.1	11.0
		4.9 ± 0.9	−6.5 ± 0.1	0.5 ± 0.1	9.09
		18.5 ± 0.9	−6.6 ± 0.1	1.3 ± 0.1	13.4
		12.2 ± 0.9	−6.2 ± 0.1	0.3 ± 0.1	41.4
		1.2 ± 0.9	−4.9 ± 0.1	0.4 ± 0.1	2.68
20350+4126	–2.5[b]	0.20 ± 0.03	−10.93 ± 0.08	0.9 ± 0.2	0.206
		0.09 ± 0.02	−4.07 ± 0.04	0.31 ± 0.07	0.268
21306+5540*	–71.1[f]	0.13 ± 0.02	−78.27 ± 0.05	0.6 ± 0.1	0.22
		0.38 ± 0.02	−73.33 ± 0.01	0.36 ± 0.02	1.01
		0.49 ± 0.03	−71.04 ± 0.02	0.69 ± 0.06	0.66
		0.47 ± 0.03	−69.90 ± 0.01	0.46 ± 0.04	0.95
		0.20 ± 0.03	−68.66 ± 0.08	1.0 ± 0.2	0.2
22272+6358	–9.9	0.46 ± 0.02	−12.880 ± 0.008	0.30 ± 0.02	1.43
		0.37 ± 0.02	−12.40 ± 0.02	0.41 ± 0.03	0.853
		20.78 ± 0.02	−11.010 ± 0.003	0.367 ± 0.003	53.1
		6.03 ± 0.02	−10.270 ± 0.001	0.372 ± 0.002	15.2
22506+5944	–51.5	0.17 ± 0.04	−55.6 ± 0.1	0.9 ± 0.3	0.172
		0.81 ± 0.02	−53.880 ± 0.006	0.44 ± 0.01	1.72
22543+6145*	–11.1[c]	71 ± 1	−4.7 ± 0.1	0.6 ± 0.1	147
		129 ± 1	−4.1 ± 0.1	0.3 ± 0.1	361
		101 ± 1	−3.8 ± 0.1	0.2 ± 0.1	394
		156 ± 1	−2.5 ± 0.1	0.5 ± 0.1	296
		30 ± 1	−1.8 ± 0.1	0.3 ± 0.1	92

Notes. [(*)] Sources rejected by Palla et al. (1991); [(a)] from Molinari et al. (1996) except when differently specified; [(b)] from NH_3 observations performed with the Nobeyama 45-m telescope simultaneously to the CH_3OH maser observations; [(c)] from CS (2–1) observations, Bronfman et al. (1996); [(d)] from Sridharan et al. (2002); [(e)] from Richards et al. (1987); [(f)] from Sunada et al. (2007) and references therein.

Table B.3. Same as Table B.2 for *low* sources.

Source	V_{LSR}[a] (km s^{-1})	$\int F_\nu dV$ (Jy km s^{-1})	V (km s^{-1})	ΔV (km s^{-1})	F_{peak} (Jy)
05137+3919	–25.4	0.21 ± 0.06	−16.2 ± 0.1	0.6 ± 0.2	0.3
06099+1800*	7.1[f]	1.8 ± 0.9	1.9 ± 0.1	0.6 ± 0.1	2.8
		5.1 ± 0.9	4.0 ± 0.1	0.3 ± 0.1	15.9
		28.7 ± 0.9	4.6 ± 0.1	0.4 ± 0.1	63.6
		15.6 ± 0.9	5.4 ± 0.1	0.4 ± 0.1	35.4
17450-2742	–16.9	0.39 ± 0.02	−12.15 ± 0.01	0.37 ± 0.03	0.986
18024-2119	0.5	25 ± 4	−5.33 ± 0.03	0.42 ± 0.08	56.0
		67 ± 3	−4.29 ± 0.07	0.8 ± 0.2	78.9
		28 ± 2	−3.81 ± 0.02	0.32 ± 0.05	83.9
		39 ± 2	−3.22 ± 0.03	0.50 ± 0.07	73.4
		27 ± 2	−5.3 ± 0.1	0.5 ± 0.1	55.4
		48 ± 2	−4.4 ± 0.1	0.6 ± 0.1	74.2
		51 ± 2	−3.8 ± 0.1	0.5 ± 0.1	105.
		33 ± 2	−3.2 ± 0.1	0.4 ± 0.1	76.5
		5 ± 2	−2.6 ± 0.1	0.6 ± 0.1	8.65
		6.2 ± 0.3	−0.827 ± 0.004	0.86 ± 0.06	6.75
		10.7 ± 0.2	−9.90.09 ± 0.006	0.62 ± 0.01	16.1
		54.3 ± 0.3	1.891 ± 0.004	1.066 ± 0.009	47.9
		24.4 ± 0.1	2.69 ± 0.01	1.29 ± 0.03	17.7
18144-1723	47.3	1.40 ± 0.04	47.510 ± 0.005	0.43 ± 0.01	3.04
		8.95 ± 0.04	49.020 ± 0.003	0.464 ± 0.003	18.1
		6.35 ± 0.04	49.600 ± 0.003	0.355 ± 0.003	16.8
		2.18 ± 0.03	50.330 ± 0.004	0.464 ± 0.007	4.42
		12.51 ± 0.03	51.090 ± 0.003	0.479 ± 0.003	24.5
		1.50 ± 0.02	51.900 ± 0.003	0.344 ± 0.006	4.10
18181-1534	–5.8[b]	1.61 ± 0.03	–3.740 ± 0.002	0.296 ± 0.006	5.1
		20.06 ± 0.03	–2.999 ± 0.003	0.399 ± 0.003	47.2
18224-1228	48.8[b]	2.14 ± 0.02	38.700 ± 0.002	0.394 ± 0.005	5.1
		0.08 ± 0.01	39.60 ± 0.02	0.19 ± 0.04	0.401
18278-1009	93.7	0.07 ± 0.02	108.70 ± 0.02	0.19 ± 0.09	0.35
		0.45 ± 0.02	109.800 ± 0.007	0.35 ± 0.02	1.19
		0.46 ± 0.02	110.900 ± 0.005	0.30 ± 0.01	1.46
		1.7 ± 0.2	115.9 ± 0.1	1.1 ± 0.1	1.48
		2.5 ± 0.2	116.5 ± 0.1	0.5 ± 0.1	4.46
		5.4 ± 0.2	117.2 ± 0.1	0.5 ± 0.1	9.98
		1.1 ± 0.2	117.9 ± 0.1	0.4 ± 0.1	2.50
	93.7	0.4 ± 0.2	118.4 ± 0.1	0.3 ± 0.1	1.13
		1.24 ± 0.02	119.000 ± 0.003	0.405 ± 0.009	2.88
		0.86 ± 0.04	119.600 ± 0.007	0.39 ± 0.02	2.08
		0.22 ± 0.04	120.20 ± 0.05	0.5 ± 0.1	0.381
18441-0134	57.6[b]	0.22 ± 0.07	78.0 ± 0.1	0.2 ± 0.1	1.02
		2.05 ± 0.07	79.2 ± 0.1	0.8 ± 0.1	2.54
		3.53 ± 0.07	80.9 ± 0.1	1.1 ± 0.1	3.04
		0.36 ± 0.02	83.080 ± 0.005	0.26 ± 0.01	1.31
		0.35 ± 0.02	83.870 ± 0.009	0.35 ± 0.02	0.946
18511+0146	56.8	0.12 ± 0.02	59.74 ± 0.03	0.42 ± 0.08	0.27626
18527+0301	76.0	3.6 ± 0.3	70.3 ± 0.1	0.6 ± 0.1	5.78
		2.0 ± 0.3	71.9 ± 0.1	0.6 ± 0.1	3.00
		10.1 ± 0.3	72.8 ± 0.1	0.7 ± 0.1	14.4
		9.1 ± 0.3	74.3 ± 0.1	0.5 ± 0.1	18.2
		0.8 ± 0.3	76.1 ± 0.1	0.4 ± 0.1	2.02
		1.06 ± 0.08	81.4 ± 0.1	0.6 ± 0.1	1.55
		1.32 ± 0.08	82.1 ± 0.1	0.4 ± 0.1	3.29
		2.64 ± 0.08	83.9 ± 0.1	0.7 ± 0.1	3.78
19012+0505	40.4	0.32 ± 0.04	31.95 ± 0.06	1.2 ± 0.2	0.243
19092+0841	58.0	3.7 ± 0.09	54.8 ± 0.1	0.6 ± 0.1	6.31
		0.56 ± 0.09	55.5 ± 0.1	0.4 ± 0.1	1.49
		0.61 ± 0.09	56.2 ± 0.1	0.4 ± 0.1	1.34
		0.84 ± 0.09	56.8 ± 0.1	0.6 ± 0.1	1.24
		0.16 ± 0.09	58.1 ± 0.1	0.3 ± 0.1	0.539
		1.67 ± 0.04	62.440 ± 0.009	0.96 ± 0.03	1.63

Table B.3. continued.

Source	V_{LSR}[a] (km s^{-1})	$\int F_\nu dV$ (Jy km s^{-1})	V (km s^{-1})	ΔV (km s^{-1})	F_{peak} (Jy)
19120+1148	55.0	0.16 ± 0.02	57.96 ± 0.04	0.6 ± 0.1	0.251
		0.21 ± 0.02	59.00 ± 0.01	0.39 ± 0.05	0.519
		0.15 ± 0.03	62.11 ± 0.09	1.0 ± 0.2	0.141
19186+1440	–	0.47 ± 0.02	–26.670 ± 0.007	0.33 ± 0.02	1.33
		1.37 ± 0.03	–25.800 ± 0.008	0.79 ± 0.02	1.62
		0.18 ± 0.05	–23.99 ± 0.08	0.9 ± 0.5	0.185
		0.92 ± 0.07	–14.86 ± 0.03	0.78 ± 0.06	1.11
		0.75 ± 0.06	–14.370 ± 0.006	0.37 ± 0.01	1.90
		2.52 ± 0.03	–13.380 ± 0.003	0.677 ± 0.008	3.50
		3.15 ± 0.03	–12.110 ± 0.003	0.698 ± 0.006	4.24
		2.97 ± 0.03	–10.750 ± 0.004	1.00 ± 0.01	2.80
22187+5559	–45.2[e]	0.09 ± 0.03	–11.44 ± 0.08	0.6 ± 0.3	0.133

Table B.4. Parameters of the 44 GHz CH_3OH maser (Class I) detected with the Nobeyama 45-m telescope for both *high* (the IRAS name begins with H) and *low* (the IRAS name is begins with L) sources.

Source[a]	V_{LSR} (km s^{-1})	$\int F_\nu dV$ (Jy km s^{-1})	V (km s^{-1})	ΔV (km s^{-1})	F_ν^{peak} (Jy)
H05168+3634	–15.1	1.12 ± 0.2	–4.9 ± 0.2	1.3 ± 0.4	0.80
H05480+2545	–9.3[b]	3.3 ± 0.1	–9.79 ± 0.02	0.77 ± 0.05	4.08
H06103+3030	15.6	2.7 ± 0.6	16.4 ± 0.7	5 ± 1.5	0.51
H18089-1732	32.9	10.9 ± 0.4	31.94 ± 0.01	0.86 ± 0.04	11.8
H18151-1208	32.8	2.2 ± 0.2	30.5 ± 0.1	1.5 ± 0.3	1.34
		2.0 ± 0.4	33.8 ± 0.2	2.1 ± 0.5	0.89
H18159-1648	22.1	4.0 ± 0.6	13.2 ± 0.1	0.9 ± 0.1	3.95
		10.9 ± 0.6	19.5 ± 0.1	1.0 ± 0.1	10.01
		15.8 ± 0.6	20.9 ± 0.1	1.0 ± 0.1	6.97
		31.4 ± 0.6	22.9 ± 0.1	0.9 ± 0.1	32.11
		18.5 ± 0.6	23.9 ± 0.1	0.6 ± 0.1	27.9
H18316-0602	42.2	6.6 ± 0.1	42.060 ± 0.008	0.62 ± 0.02	9.88
		1.6 ± 0.2	43.10 ± 0.04	0.70 ± 0.09	2.07
		2.9 ± 0.4	44.52 ± 0.09	1.6 ± 0.3	1.67
H18360-0537	102.3	6.7 ± 0.4	102.4 ± 0.1	2.83 ± 0.2	2.23
		1.6 ± 0.4	106.4 ± 0.3	1.9 ± 0.7	0.74
H18507+0121	57.1	10.0 ± 0.4	60.33 ± 0.04	1.3 ± 0.1	7.00
H18517+0437	43.7	3.1 ± 0.2	43.97 ± 0.05	1.1 ± 0.1	2.70
H19043+0726	58.9	2.5 ± 0.2	58.69 ± 0.03	0.65 ± 0.09	3.52
		1.1 ± 0.2	59.89 ± 0.08	0.7 ± 0.2	1.31
H19088+0902	59.6	10 ± 1	58.67 ± 0.07	2.2 ± 0.2	2.0
H19388+2357	34.6	1.8 ± 0.4	35.4 ± 0.2	1.6 ± 0.4	1.07
H20050+2720	6.4	2.0 ± 0.2	6.6 ± 0.1	1.8 ± 0.3	1.09
H20062+3550	0.6	2.5 ± 0.2	0.60 ± 0.06	1.0 ± 0.1	2.36
H20126+4104	–3.9	8.9 ± 0.4	–2.43 ± 0.04	2.0 ± 0.1	4.17
H20188+3928	1.5	2 ± 1	3 ± 1	3 ± 2	0.76
H21391+5802	0.4	4.2 ± 0.2	–0.49 ± 0.02	0.73 ± 0.08	5.33
		5.4 ± 0.4	6.6 ± 0.1	2.3 ± 0.3	2.25
H22506+5944	–51.5	3 ± 1	–51.3 ± 0.1	1.6 ± 0.6	1.81
		4 ± 2	–48 ± 1	5 ± 2	0.8
L00420+5530	–51.20	1.6 ± 0.4	–48.8 ± 0.3	2.0 ± 0.5	0.8
L18018-2426	10.5	241.1 ± 0.4	11.280 ± 0.003	0.669 ± 0.002	339
L18024-2119	0.5	10.0 ± 0.4	0.31 ± 0.02	1.28 ± 0.05	7.34
		3.1 ± 0.4	2.7 ± 0.1	2.3 ± 0.3	1.4
L18144-1723	47.3	42.1 ± 0.2	48.590 ± 0.005	1.54 ± 0.01	25.6
L18162-1612	61.8	5.1 ± 0.2	62.80 ± 0.03	0.84 ± 0.07	3.2
L18396-0431	97.3	1.0 ± 0.2	97.6 ± 0.1	1.0 ± 0.3	1.0
L19092+0841	58.0	4.0 ± 0.4	59.07 ± 0.4	5.7 ± 0.7	0.65
L23385+6053	–50.0	2.9 ± 0.4	–50.6 ± 0.3	3.2 ± 0.7	0.9

Notes. [(a)] "L" and "H" indicate if the source belongs to the *low* or *high* sample; [(b)] from NH_3 observations performed with the Nobeyama 45-m telescope.

Table B.5. Same as Table B.4 for the 95 GHz CH_3OH maser (Class I) detected with the Nobeyama 45-m telescope.

Source[a]	V_{LSR} (km s^{-1})	$\int F_\nu dV$ (Jy km s^{-1})	V (km s^{-1})	ΔV (km s^{-1})	F_ν^{peak} (Jy)
H05480+2545	–9.3[b]	3.1 ± 0.6	–10.6 ± 0.1	1.3 ± 0.3	2.2
H18089-1732	32.9	2.7 ± 0.4	31.38 ± 0.02	0.45 ± 0.05	5.5
		14 ± 2	32.4 ± 0.2	3.2 ± 0.4	4.2
H18159-1648	22.1	4.7 ± 0.8	20.1 ± 0.1	1.6 ± 0.4	2.7
		7.6 ± 0.6	22.56 ± 0.06	1.4 ± 0.1	5.2
H18316-0602	42.2	1.1 ± 0.2	41.63 ± 0.05	0.5 ± 0.1	2.1
H18360-0537	102.3	13.2 ± 0.8	102.5 ± 0.1	4.1 ± 0.4	4.0
H20126+4104	–3.9	6.0 ± 0.4	–2.75 ± 0.08	2.3 ± 0.2	2.5
H21391+5802	0.4	2.5 ± 0.6	12.1 ± 0.1	1.2 ± 0.5	2.0
H22506+5944	–51.5	5 ± 1	–47.1 ± 0.2	2.4 ± 0.6	2.0
L18018-2426	10.5	33.5 ± 0.4	10.800 ± 0.004	0.622 ± 0.009	50
L18144-1723	47.3	26.4 ± 0.6	47.91 ± 0.03	2.07 ± 0.08	12
L18396-0431	97.3	3.8 ± 0.4	50.37 ± 0.08	1.24 ± 0.2	2.9
		14 ± 2	57.4 ± 0.6	7 ± 1	1.9
		4 ± 1	61.5 ± 0.1	1.3 ± 0.4	2.5
		8.0 ± 0.8	71.3 ± 0.2	3.4 ± 0.6	2.2
		1.6 ± 0.2	130.50 ± 0.08	0.7 ± 0.1	2.1

Notes. [a] "L" and "H" indicate if the source belongs to the *low* or *high* sample; [b] from NH_3 observations performed with the Nobeyama 45-m telescope.